JGR Oceans

Key Points:

- The mixed layers and mode waters are identified by inspecting the shape of each profile
- Two types of the South Atlantic Subtropical Mode Water originate at the Agulhas Leakage
- Anticyclonic eddies hold more and thicker mode water layers than cyclonic eddies

Correspondence to:
Y. Chen,
yanxu.chen@lmd.ens.fr

Formation and Transport of the South Atlantic Subtropical Mode Water in Eddy-Permitting Observations

Yanxu Chen[1] [ID], **Sabrina Speich[1]** [ID], **and Rémi Laxenaire[1,2]** [ID]

[1]Laboratoire de Météorologie Dynamique (IPSL), Ecole Normale Supérieure (PSL), Paris, France, [2]Center for Ocean-Atmospheric Prediction Studies, Florida State University, Tallahassee, FL, USA

Abstract We present in this study a detecting algorithm that enables to identify both the ocean surface mixed layer depth (MLD) and mode water from the Argo profiling data. This algorithm proposes a detection based on the calculation of the first and second derivatives for each temperature (or density) profile. Low gradients reveal segments of water mass homogeneity, while extreme values of second derivatives indicate the precise depths at which the gradients sharply change. Specifically applied to detect the South Atlantic Subtropical Mode Water (SASTMW), this algorithm leads to a redefinition of the three mode water types discussed in Sato and Polito (2014; https://doi.org/10.1002/2013JC009438) as well as new insights into the origins of these water masses and their dynamics. In particular, we point out that only one of the SASTMW varieties originates from the Brazil-Malvinas Confluence in the western boundary, whereas the other two are related to the Agulhas Leakage that shapes the Indo-Atlantic water mass exchanges. As both regions of the SASTMW formation are characterized by intense eddy kinetic energy, the role of mesoscale eddies in the SASTMW formation and transport is also investigated by co-locating Argo profiles with eddies objectively identified from satellite altimetry maps. It suggests that anticyclonic eddies correspond to a larger number and thicker layers of SASTMW than their cyclonic counterparts. In the Cape Basin, where mode waters are found correlated with the main paths of Agulhas Rings, a potential route of subduction is also proposed.

Plain Language Summary Mode waters are essential components in the upper ocean, of which the spatial and temporal variability significantly contributes to the large-scale climate dynamics. This contribution can be inferred from the weakly stratified characteristics of mode waters that are formed due to winter surface cooling. Regarding the homogeneity of both surface mixed layers and mode waters, we developed a general statistical algorithm to detect their presence from different observational profiling platforms. Argo floats are one of these platforms that drift up and down to retrieve temperature and salinity profiles. Therefore in this study, one attempt is to apply the detecting algorithm to Argo profiles in the South Atlantic subtropics. The novelty of this diagnostic algorithm lies in a precise inspection that results from the searching of variations in each individual profile, instead of implementing universal thresholds for all. Combined with satellite-derived eddy detecting methods, the effect of mesoscale eddies on mode water formation and transport is quantified and might further shed light on other regional and basin-scale mode water dynamics. This combination is also helpful to show how mode waters modulate the ocean state acting in response to changes such as an increasing oceanic uptake of anthropogenic heat and CO_2.

1. Introduction

As the largest heat reservoir in the Earth system, the ocean mediates climate variations by directly sequestering CO_2 (DeVries, 2014; Friedlingstein et al., 2020; Sabine et al., 2004) and taking up about 90% of the radiative imbalance due to this anthropogenic interference (Cheng et al., 2017; Levitus et al., 2012; von Schuckmann et al., 2020). The spatio-temporal variability of such heat and CO_2 uptake and storage is dependent on various physical mechanisms from both ocean surface and subsurface perspectives. Intuitively, air-sea heat and momentum fluxes generate and modulate sea surface temperature (SST) anomalies, which in turn, provide feedback to these fluxes (Park et al., 2005). In addition, studies have also observed and examined a reemergence mechanism of SST anomalies from one winter to another, without maintaining through the summer in between (Alexander & Deser, 1995; Deser et al., 2003; Hanawa & Sugimoto, 2004). Such reemergence has been linked to the presence of mode waters capped underneath the seasonal thermocline and characterized by a substantial volume of thermostad or pycnostad (a layer with low temperature or density gradients) distributed broadly in the ocean interior (Hanawa & Talley, 2001; Speer & Forget, 2013). The dynamical nature of mode waters is thus often

linked to surface buoyancy loss and accordingly thought of as memories of previous atmospheric forcing (Bates et al., 2002; Davis et al., 2011; Yasuda & Hanawa, 1997), and could potentially reproduce these memories, for example, by modulating regional and remote heat content and driving SST anomalies in following years.

Despite the large area occupied by mode waters, their formation is much more bounded to specific locations. In particular, the Subtropical Mode Water (STMW) has been documented to originate, in common cases, in the vicinity of western boundary currents, where surface waters lose buoyancy in winter and deep mixed layer develops due to convection. Part of this winter mixed layer is later capped by heating and isolated from the surface while circulating in the subtropical gyres, and might eventually subduct (Marshall, 1997). Of all the five subtropical gyres, STMW is thus commonly divided into three varieties in terms of formation zones and thermodynamic characteristics: the one that has a western-boundary origin of formation (e.g., Kwon & Riser, 2004; Roemmich & Cornuelle, 1992; Suga & Hanawa, 1990; Tsubouchi et al., 2016), the one linked to the downstream transport and subduction along the poleward boundary of the subtropical gyre (Nakamura, 1996; Oka et al., 2011), and a third variety that appears in the eastern extremity of gyres, which is sometimes influenced by inter-basin exchanges of water masses (de Souza et al., 2018; Hautala & Roemmich, 1998; Wong & Johnson, 2003).

Since the formation and transport of mode water are highly dependent on the seasonal variability of mixed layer depth (MLD) while the transfer of mass, momentum, and energy across the mixed layer provides the source of almost all motions in the ocean, it is crucial to properly identify MLD and to accurately detect mode water at depth from observations. The most widely employed methods of MLD detection rely on a predefined threshold of temperature or density changes between a reference depth at the surface and the bottom of the mixed layer (de Boyer Montégut et al., 2004; Kara et al., 2000), or a critical gradient threshold that the base of mixed layer might satisfy (Dong et al., 2008). Simple to apply, nonetheless, these methods are limited in that it is difficult to decide on a single criterion for all profiles in the world ocean. Based on these methods, Holte and Talley (2009) developed a hybrid algorithm to select the best MLD estimates and the greatest utility of their algorithm lies in its ability to work with temperature-only profiles. This hybrid MLD selection was employed by Schmidtko et al. (2013) to construct a global isopycnal upper-ocean climatology, applied by Gaube et al. (2019) in examining the effect of mesoscale eddies on the modulation of MLD, and commonly used to compare with numerical results (Bachman et al., 2017). Here, considering the homogeneity of both surface mixed layers and mode waters, we propose a new algorithm that uses the conditions of both the gradients and second derivatives to diagnose vertical features. Low gradients reveal segments of water mass homogeneity, while extreme values of second derivatives indicate the precise depths at which the gradients sharply change. A similar detection applied to historical hydrographic profiling data was developed by Lorbacher et al. (2006) that sought for the shallowest extreme curvature as the MLD. Details of this new algorithm and its application to the Argo profiles will be described in this article.

With the progress in eddy detecting and tracking from satellite altimetry, several methods have been developed to objectively reconstruct the evolution of mesoscale eddies over time (Chaigneau et al., 2011; Chelton et al., 2011; Laxenaire et al., 2018; Pegliasco et al., 2015; Vu et al., 2018). Combining the results of eddy-permitting models with observed diagnoses, it is widely accepted that mesoscale eddies make a substantial contribution to mode water dynamics, including the formation of deep winter mixed layer that is closely associated with anticyclonic eddies (Dufois et al., 2016; Kouketsu et al., 2012; Uehara et al., 2003), the enhancement of mode water subduction by eddy-driven ageostrophic motions (Marshall, 1997; Nishikawa et al., 2010; Qu et al., 2002; Spall, 1995; Xu et al., 2016), and the dependence of STMW decadal variability on stability of the recirculation gyre rather than variations in air-sea fluxes (Qiu & Chen, 2006). Though some eddies evolve in the ocean interior along their trajectories, very often signatures are generated at the surface that can still be detected by satellites (Bashmachnikov & Carton, 2012; Laxenaire et al., 2019). In particular, Laxenaire et al. (2018) showed that a significant fraction of eddies can be followed from the Indian Ocean to the South Brazil Current with around 3.5 years to cross the entire South Atlantic. Other observations also suggest that long-lived and far-traveled subsurface eddies exhibit a preference for rapid anticyclonic rotation that leads to the isolation of core water masses (Schütte et al., 2016).

To distinguish subsurface-intensified eddies from surface ones, a recent study (Assassi et al., 2016) has proposed a simple index of distinction based on the ratio of SST anomalies and sea level anomalies (SLAs). However, this separation encounters errors when strong currents exist close to eddies, implying that the method is not feasible to identify the mode water trapping eddies that just detach from the main currents. Here in this study, we instead make use of the calculation of steric height anomaly (SHA) to separate subsurface eddies from surface ones (Gill & Niller, 1973). This method was also applied to identify pathways of eddies propagating westward in the South

Indian Ocean in Dilmahamod et al. (2018), where several generation mechanisms of subsurface eddies were also reviewed. A recent study (McCoy et al., 2020) further draws a global distribution of subsurface eddies detected from a more complex algorithm that is dependent on three criteria: spiciness as a measure of thermohaline variability, buoyancy frequency as an estimate of stratification, and finally, the dynamic height anomaly indicative of the horizontal gradient force. It is noteworthy that the dynamic height anomaly is calculated for the detection of subsurface eddies in this study, while the other two criteria are more or less equivalent to our mode water detecting algorithm.

Here, we specifically validate the algorithm of MLD and mode water detection through the South Atlantic Subtropical Mode Water (SASTMW), which has received much less attention compared with the northern hemisphere oceans (Bernardo & Sato, 2020; de Souza et al., 2018; Provost et al., 1999; Sato & Polito, 2014). It is of interest to study the South Atlantic subtropics primarily for the reason that the SASTMW not only contains a typical variety that develops from the western boundary (i.e., the Brazil-Malvinas Confluence), but also includes other types that interconnect with another basin (i.e., the water mass intrusion through the Agulhas Ring Corridor from the Indian Ocean). In a nutshell, the objectives of this study are to:

1. clarify the new algorithm applied to Argo profiles to detect surface mixed layers and mode waters;
2. briefly summarize the distribution and characteristics of SASTMW detected by the algorithm, and mainly compare with Sato and Polito (2014), the most recent study of SASTMW;
3. co-locate eddy positions extracted by the satellite-deduced TOEddies algorithm (Laxenaire et al., 2018) with the Argo profiles, in an attempt to evaluate the effect of mesoscale eddies on mode water formation and transport in this region;
4. follow the SHA method that separates subsurface eddies from surface ones, and apply this separation to TOEddies algorithm to further draw possible patterns of subduction associated with mode waters.

This study is organized as follows. In the next section, the data we have used are described and the methods we have developed are introduced. Validation of the new algorithm to calculate MLD and mode water thickness is also presented, along with a summary of all STMW detection methods in the literature. Section 3 of results firstly compares our MLD detection in the South Atlantic with other simple threshold methods and the hybrid method developed by Holte and Talley (2009), and it subsequently presents a reconstruction of the SASTMW field and a reclassification into three mode water types; the reclassification allows for a closer inspection of the spatial distribution, vertical configuration and thermodynamic features of each type, providing a more quantifiable correlation with mesoscale eddies. A discussion and conclusion are followed in the last section.

2. Data and Methods

2.1. The Argo Data Set of the South Atlantic

Argo floats provide a vast array of conductivity, temperature, and depth (CTD) vertical profiles from the ocean surface down to 2,000 m (Argo, 2020). Thus, the contributions of Argo array to the ocean observing system, particularly with regard to the availability of subsurface quantities and extensive coverage of remote ocean areas, are a profound progress to characterize water masses and large-scale motions. Furthermore, these data have been widely used to make accurate estimates of heat and freshwater storage and their transport by ocean currents. Here, in this study, these profiling data were retrieved from the global TOEddies atlas (Laxenaire et al., 2019) that not only contains the detection of mesoscale eddies from closed absolute dynamic topography (ADT) contours, but also includes co-location of these detected eddies with Argo profiles. In the original TOEddies atlas, some selections were made to use the delayed mode Argo data available at the Coriolis Global Data Center (Coriolis GDAC; http://www.coriolis.eu.org) with quality control flags equal to 1 and 2, which refer to "good observation" and "probably good observation". These selections then involved a preference of minimum vertical resolution for several depth ranges, and enough observations at the surface and deeper than 1,200 m (more details in Laxenaire et al., 2020). The data of profiles satisfying all these criteria are interpolated vertically at a 10-m depth step eventually.

The South Atlantic region of interest is bounded from the equator to 60°S in the latitude direction, and assumed to extend from the entire subtropical gyre system to the formation area of Agulhas Rings longitudinally (70°W–30°E), including 122,202 profiles in total between years 2000 and 2018, as shown in Figure 1. The
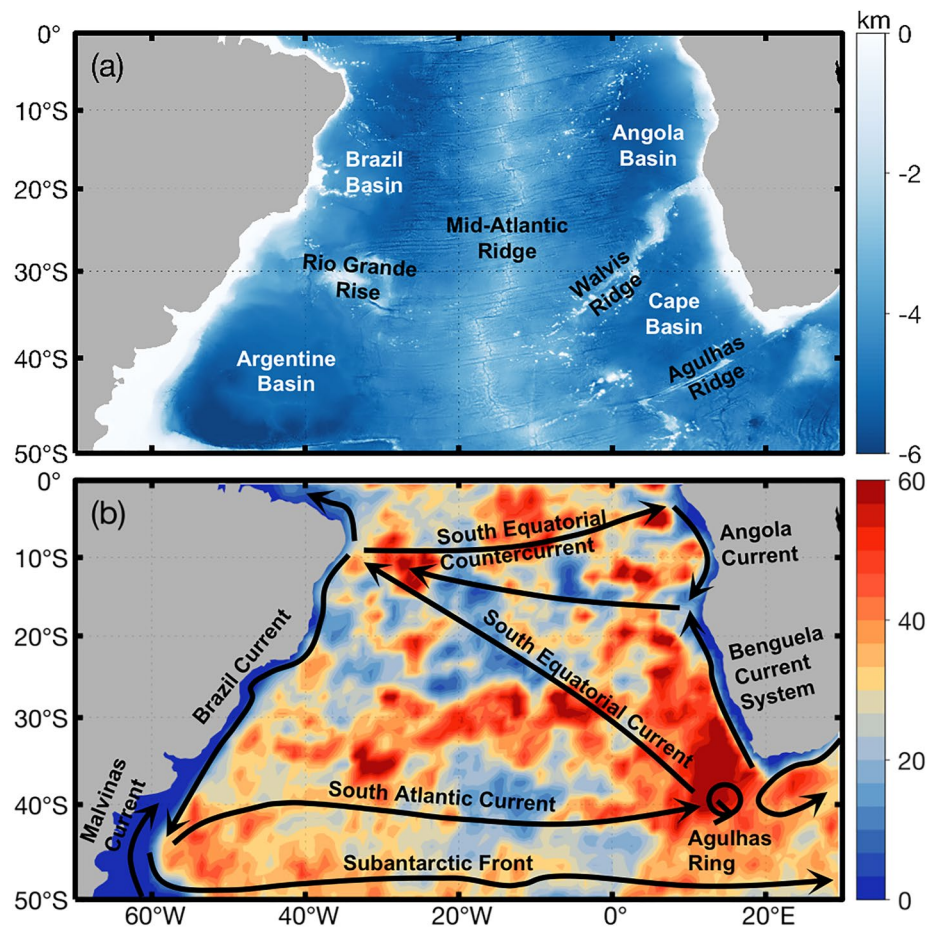
Figure 1. The area of study including (a) bathymetry from the ETOPO2 dataset (Smith & Sandwell, 1997) and (b) spatial distribution of Argo profiles in the South Atlantic between years 2000 and 2018, superposed by the main surface circulation structures (the South Atlantic subtropical gyre, limited by the South Equatorial Current at its equatorward limit, the Benguela Current system at its eastern limit, the Agulhas Current Retroflection and Agulhas Rings at its southeastern end, the Circumpolar Current at its southern frontiers, the Brazil-Malvinas Confluence at its southwestern end and the South Brazil Current materializing its western boundary). The schematic of surface circulation is manually drawn in accordance with the overview of the South Atlantic circulation pattern in Talley et al. (2011). The number of profiles is counted in each 1° × 1° grid and then smoothed by a Gaussian filter of 3° in space.

number of profiles has greatly increased since 2004, due to additional deployments of floats (e.g., the histogram from Figure 1 in Sato and Polito, 2014). Since the actual float trajectories are affected by currents and smaller-scale motions, the spatial distribution of profiles as counted in each 1° × 1° grid shown in Figure 1b remains subject to the dynamical patterns, with a hotspot area in the turbulent Cape Basin where the Agulhas Rings are formed.

2.2. The Detection Algorithm of the Mixed Layer and Mode Water

In brief, this algorithm first interpolates each profile's properties at equal pressure intervals $\Delta p = 2$ dbar using the Akima spline (Akima, 1970). Subsequently, it estimates a first guess for the MLD by searching for the extreme curvature (Lorbacher et al., 2006 used the word "curvature" to relate to the second derivative in calculus. In this article, we follow this diction) of density profile that is located above the extreme gradient. This first estimate is then validated by the density threshold of difference as applied in previous studies of the mixed layer detection. Instead of a derivation from density as the MLD, the identification of mode water is based on temperature profiles. Here, we consider two vertical configurations of mode water, counting both (a) outcropping mode waters that capture the processes of formation or renewal close to the western boundary currents and adjacent areas, as
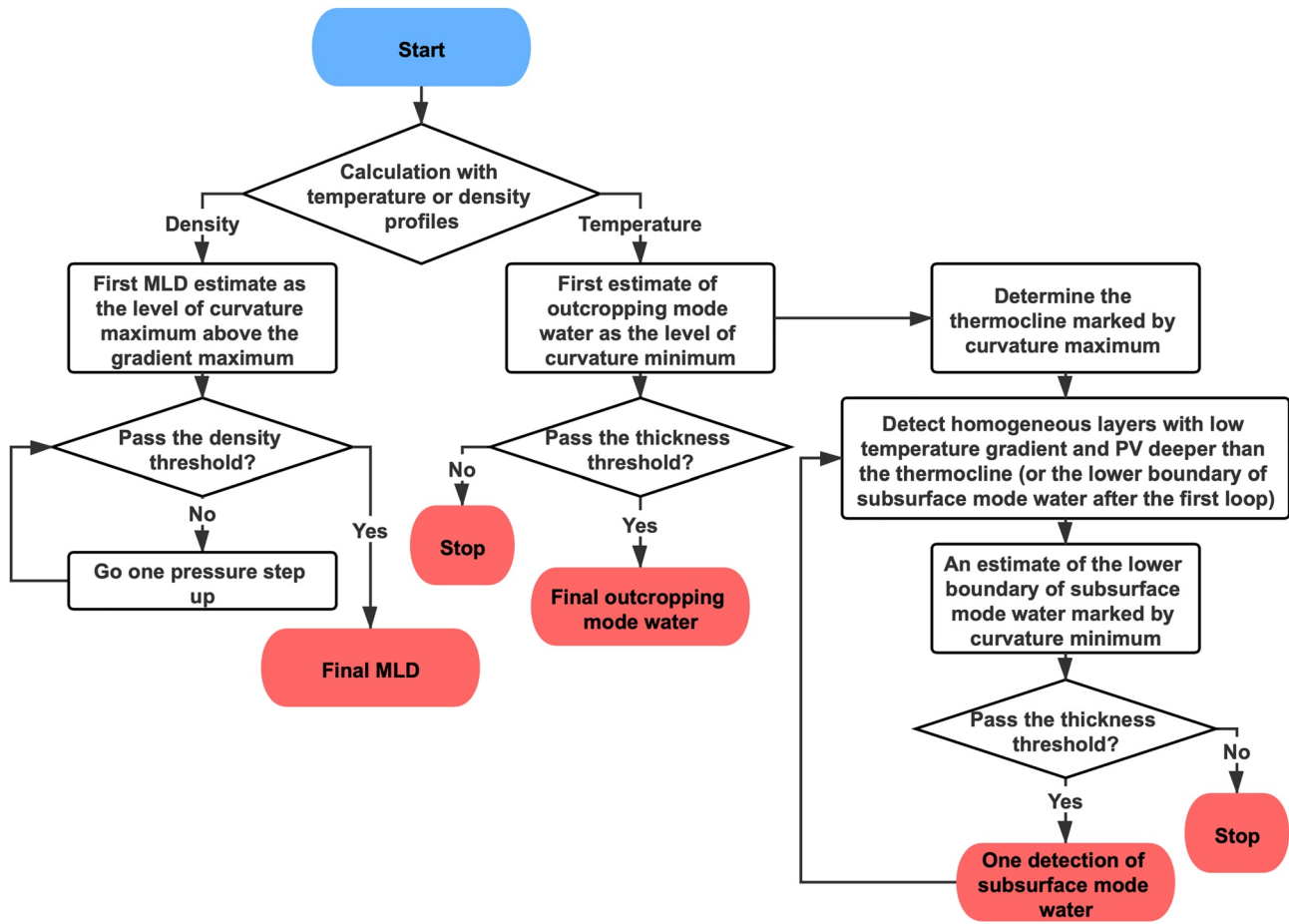
Figure 2. Flowchart of the mixed layer depth (MLD) and mode water detecting algorithm to precisely capture the depths and thicknesses associated with these homogeneous layers. While the MLD calculation is based on density, mode waters are identified as thick thermostads.

well as the influence of Indo-Atlantic water exchanges; and (b) subsurface mode waters identified as thick thermostads underneath the seasonal thermocline, implying possible histories of subduction. The detailed description of our approach is provided below accompanied by a flowchart of processes (Figure 2) and three typical profile examples discerned with mode water layers by the algorithm in the subtropical South Atlantic (Figure 3).

The detecting algorithm starts with calculations of gradient and curvature profiles. We denote $i = 1$ as the level closest to the surface, then the gradient of the vertical profile at level i is defined by central difference

$$g_{\sigma_0}(i) = \frac{\sigma_0(i+1) - \sigma_0(i-1)}{2\Delta p}, \tag{1}$$

where the indication σ_0 as potential density (1,000 kg m^{-3} was subtracted from the potential density to produce sigma units) could be switched to θ as potential temperature. Accordingly, the algorithm works for both temperature and density profiles. Also note that the subscript i varies between 2 and $n - 1$ with n indicating the length of the profile. This method computes values along the edges of the profile with single-sided differences, $g_{\sigma_0}(1) = [\sigma_0(2) - \sigma_0(1)]/\Delta p$ and $g_{\sigma_0}(n) = [\sigma_0(n) - \sigma_0(n-1)]/\Delta p$, where g_{σ_0} is positive since potential density commonly increases with pressure while g_{θ} is conversely negative. Then the curvature is given by

$$c_{\sigma_0}(i) = \frac{g_{\sigma_0}(i+1) - g_{\sigma_0}(i-1)}{2\Delta p}, \tag{2}$$

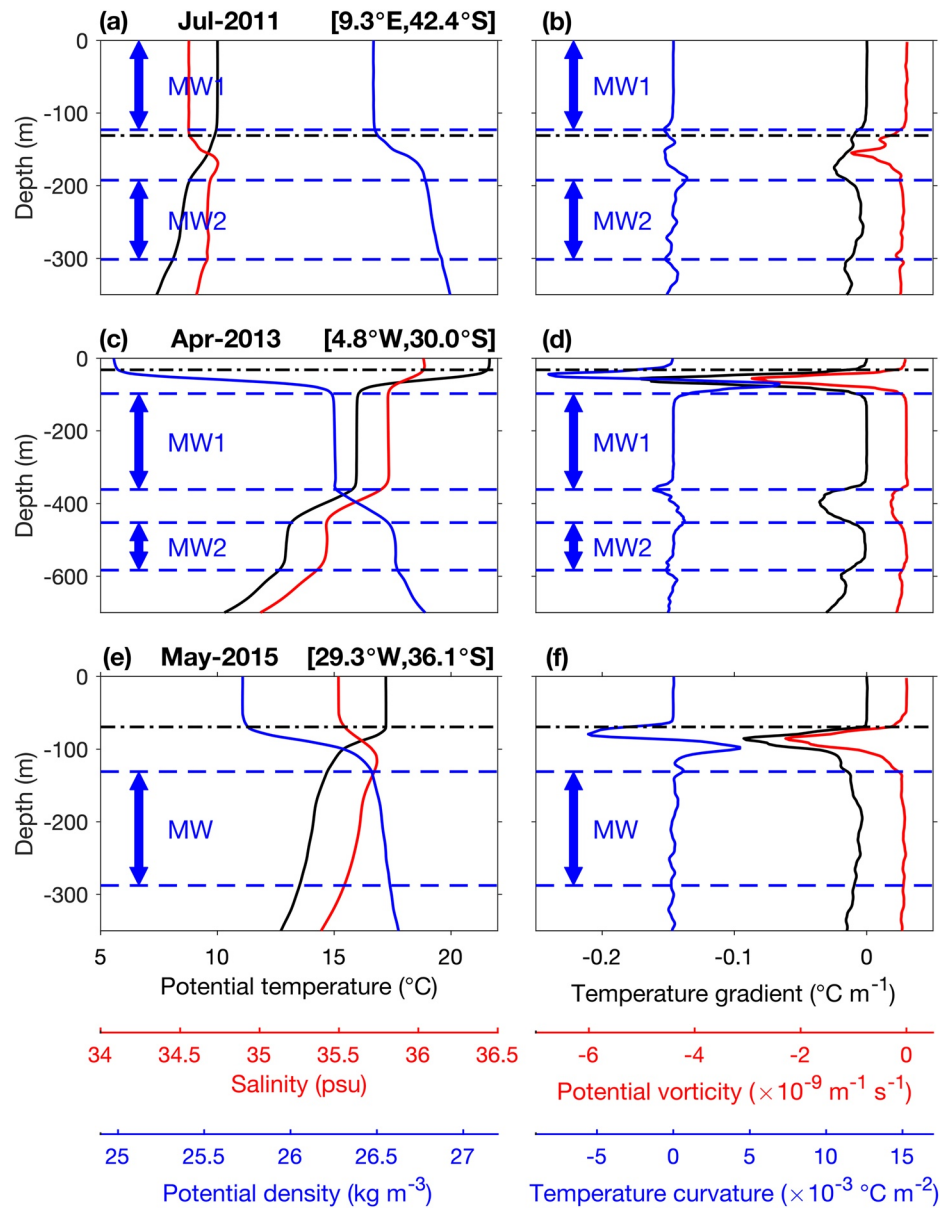where the values at edges also follow single-sided calculations.

Figure 3. Three Argo profile examples of the mixed layer depth (MLD) and mode water detection. The left panels show profiles of potential temperature, salinity, and potential density. The right panels show profiles of temperature gradient, potential vorticity, and temperature curvature. The black dash-dot lines indicate the final estimates of MLD and the extent between the two blue dashed lines in each panel is a potential presence of mode water. The profile (c/d) is co-located with an anticyclonic Agulhas Ring detected from TOEddies algorithm (Laxenaire et al., 2019), and has been identified as a subsurface eddy from the calculation of steric height anomaly (SHA). Profiles (a/b) and (e/f) are not detected as eddies from the altimetry, but these two profiles display a maximum SHA in the subsurface and at the surface, respectively (The possibility of eddy detection by the calculation of SHA alone is discussed in Appendix A).

In this study, while the detection of mode water is based on temperature, the MLD is alternatively estimated from density profiles. One of the reasons is the phenomena of barrier layers that are typically found in tropical regions or near river mouths (Sato et al., 2006; Sprintall & Tomczak, 1992). These barrier layers are named given the conditions of a thick thermostad layer that coexists with a shallower stratification in salinity, and thus are defined by the discrepancy between a deeper temperature-based mixed layer and a thinner density-based mixed layer. Specifically in the South Atlantic tropical region, the barrier layer occurrence rate and thickness are higher at a latitude band centered around 10°S and located at the western side of the basin (e.g., Figure 1 in Sato et al., 2006). With a focus on well-mixed properties of the surface, density profiles are accordingly used to detect the MLD.
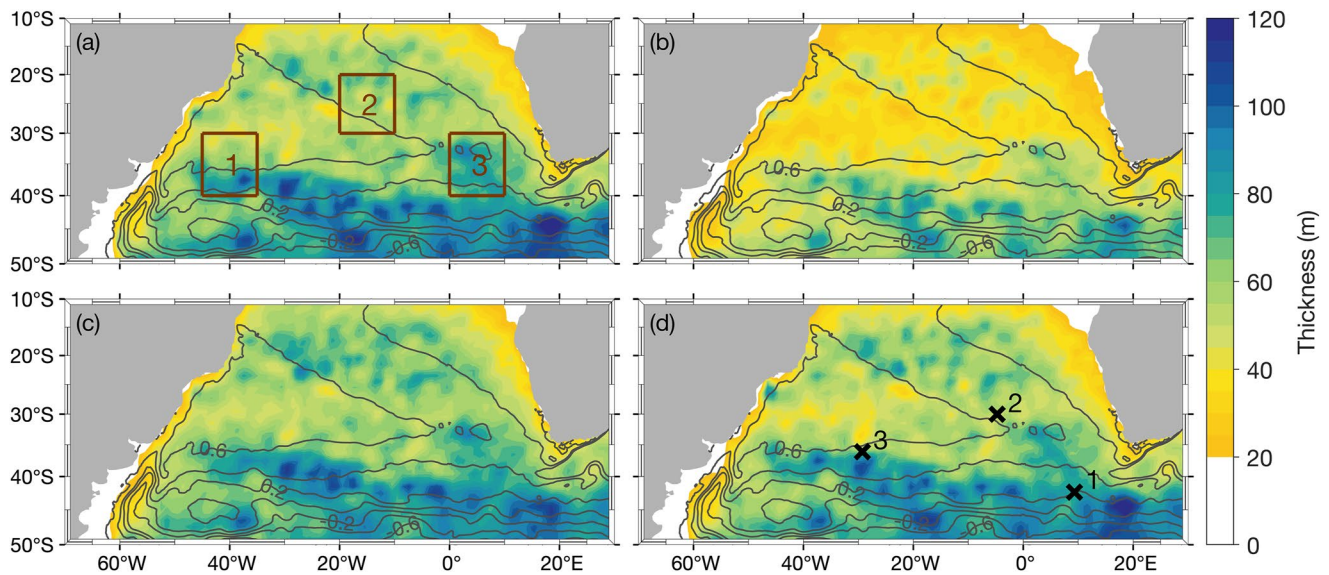
Figure 4. Maximum mixed layer depths (MLDs) detected with four different methods (calculated as mean values of five MLD maximums in each grid box of each year, and then averaged over years 2000–2018). Four panels show MLD detection by (a) density threshold; (b) density gradient threshold; (c) the hybrid method applied to density profiles developed by Holte and Talley (2009); (d) the new method dependent on the gradients and curvatures of each single profile. These maps of MLD were smoothed by a Gaussian filter of 3° in space. MLDs with thicknesses less than 20 m were removed. Brown squares in (a) display three 10° × 10° domains to compare the four methods in detail, as summarized in Table 2. The three black crosses in (d) locate the profile examples shown in Figure 3. The overlapping gray contours indicate the mean dynamic topography (MDT) as an estimate of the mean sea surface height above geoid over the 1993–2012 period (Mulet et al., 2021). These MDT contours are used to provide the mean structure of the upper-ocean mean circulation, positioning the limits of the South Atlantic subtropical gyre, the Agulhas Current Retroflection south of Africa, the Antarctic Circumpolar Current, the Brazil-Malvinas Confluence region, and the Zapiola gyre both of which are located near the South American continent (see Figure 1).

To find the pressure level closest to the bottom of the mixed layer, our next step is to select a good representative of pycnocline (or thermocline in θ profiles) that is indicated by the extreme local values of gradients. Since any pycnocline is a spanning over a depth range rather than a specific level, this detection therefore does not point to a precise diagnosis but rather a lower boundary condition for the MLD. That is, the first estimate of MLD is proposed to be the extreme local maximum of curvature above this approximate pycnocline, given that extreme values of density curvature indicate the depths at which the gradients sharply change.

To validate the MLD detection, a predefined threshold of density is introduced to check whether the density difference between the first detected MLD level and the surface reference depth is lower than this threshold value. That is to say, the density threshold works as a constraint to approve the detection of mixed layer that is homogeneous enough. The surface reference depth is chosen to be the very first one in the profile rather than 10 dbar that is more widely used in the literature, since the profiles have been interpolated in a way that already remove outliers at the very surface. In other words, this validation translates the previous threshold methods in the literature to a new application that verifies the algorithm result. Hence, we follow to set the same values of thresholds as $\sigma_{0th} = 0.03$ kg m^{-3} for density profiles and $\theta_{th} = 0.2$°C for temperature profiles summarized in de Boyer Montégut et al. (2004) and Holte and Talley (2009). If the first approximate MLD does not satisfy the validation test against the density threshold, a loop subsequently follows starting with the closest pressure level on top. The bottom boundary of pycnocline (or in some literature the pycnocline itself) can also be marked by the local minimum of curvature below the level of the extreme density gradient. Three examples are given in Figure 3, and in each panel, the black dash-dot lines indicate the density-determined MLD while the blue dashed lines represent either the upper or lower boundary of mode waters. The geographical locations of these three example profiles are also marked by crosses in the bottom right panel of Figure 4.

In theory, this gradient-dependent and curvature-dependent algorithm improves the precision of detection compared with previous MLD detecting methods based on threshold criteria. Figure 3 features the complexity of the upper ocean vertical structures in the South Atlantic, indicating that stratification depends strongly on the dynamical regions and seasons. Many other examples are also shown in other domains of the global ocean, for example, Figure 2 in Lorbacher et al. (2006). This complexity implies that a value of threshold chosen subjectively

for one region or season might not be applicable to another condition. At the same time, Lorbacher et al. (2006) recognized four systematic biases of the resulting MLD when a threshold is applied to idealized temperature profiles: the uncertainties of the threshold itself; the choices of surface reference value; vertical resolution and finally the vertical gradient at the base of the mixed layer. Another popular MLD definition takes a prescribed gradient threshold (either temperature or density) as the criterion. The fact that this gradient threshold is usually kept constant for all domains and time, likewise, makes it less robust. The method in this study, on the contrary, allows for each profile to decide on its own MLD by pinpointing the local extreme curvature (with the same set of thresholds functioning as to validate the estimates). Presumably, the first MLD detection marks a distinguished feature of the depth to which the most recent mixing process penetrates.

As summarized in the flowchart of Figure 2, the algorithm next detects mode water layers from temperature profiles. This dependence of SASTMW detection on temperature takes into account a unique vertical structure of undifferentiated density that results from the offset between temperature and salinity stratification. With this regard, mode waters with different origins can thus be separated when the detection is applied to temperature profiles instead of density. First, a similar process to the density-derived MLD detection is implemented in order to identify the outcropping mode water. Such definition can also be found in studies aimed to infer the renewal of mode waters at the sea surface with intense convection (Oka et al., 2011; Sato & Polito, 2014). Here, we define surface layers thicker than 100 dbar as potential candidates for outcropping mode waters due to their deeply homogenized thermal characteristics. This critical thickness of 100 dbar was chosen in that the mean value of all winter density-derived MLDs in the South Atlantic subtropics (averaged over June to September) reaches 92 dbar. Similar to the setting of density threshold for MLD validation, θ_{th} = 0.2°C is applied to validate the homogeneity of outcropping mode water layers from temperature profiles.

To further detect the potential presence of subsurface mode water layers, a limitation on temperature gradients is applied in addition to a typical constraint of potential vorticity (i.e., the subsurface mode water detection requires both homogeneity in temperature and density). The potential vorticity q, when relative vorticity is ignored, is estimated as $q = (f/\rho) \cdot (\partial\rho/\partial z)$, where f is the Coriolis parameter and ρ is the potential density. Any portion of the profile where $|q| <= 1.50 \times 10^{-10}$ m^{-1} s^{-1} is indicated as a candidate for mode water, while the criterion of potential temperature gradient is set to be $|g_\theta| < =0.015$°C m^{-1}. These two critical values are applicable to other domains of interest as universal criteria to detect mode waters, whilst other parameters were evaluated in Provost et al. (1999) and Sato and Polito (2014), such as restrictions on geographical location, temperature, salinity, and density ranges to specifically facilitate the detection of subtropical mode waters in the South Atlantic. To select only the SASTMW, a similar set of categories is also applied in this study, for example, a potential temperature range 11–20°C, a salinity range 34.5–36.5 psu, and a potential density range 25.5–26.8 kg m^{-3}. These values were chosen from the temperature-salinity relation of the subtropical mode waters that also conform to the selection in Sato and Polito (2014). Accordingly, the selection determined by low potential vorticity and temperature gradient searches for consecutive vertical layers exceeding 100 dbar as the total thickness that contains mode waters in between, and afterward a similar calculation to that of the mixed layer follows. That is, it then seeks the level of extreme curvature of the temperature profile and specifies this level as the lower boundary of mode water. In some special cases, two or more subsurface mode water cores are obtained using this algorithm, for example, the (c/d) profile in Figure 3 that is co-located with a subsurface-intensified anticyclonic Agulhas Ring.

This algorithm for MLD and mode water detection has also been tested with other databases, for example, temperature profiles of expendable bathythermographs (XBTs), hydrographic CTD profiles, and gridded climatologies (not shown). And to generally compare the new algorithm's applicability with mode water detecting methods for other subtropical basins, Table 1 displays a collection of methods developed in the literature. In an attempt to search for layers of weak stratification, methods based on density profiles tend to look for density gradient minimum that is approximately equivalent to searching for the lowest potential vorticity (Feucher et al., 2016; Provost et al., 1999; Sato & Polito, 2014; Xu et al., 2017), whilst methods in terms of temperature accordingly seek for a thermostad (Kwon & Riser, 2004; Roemmich & Cornuelle, 1992; Tsubouchi et al., 2007, 2010; Wu et al., 2020). For the latter, the layer with minimal temperature gradients is also referred to as the core layer of mode water and has been used to determine the upper and lower boundaries of mode water. For example, Tsubouchi et al. (2016) made a comparison of mode waters in five subtropical basins by computing the core layer temperature (CLT) that is the temperature found at the depth of gradient minimum. In each subtropical gyre, CLTs of all profiles are averaged and mode water in each profile is then defined as a window spanning over the averaged CLT ±1°C with

Table 1
Methods of Subtropical Mode Water Detection in the Global Ocean

Subtropical domains	Data in use	Methods	References
North Atlantic	Climatology (WOD2001) and profiling data (both from WOCE floats and Argo)[a]	To look for temperature gradients less than 0.006°C m^{-1}	Kwon and Riser (2004)
	Argo	To seek stratification minimum (N^2) and also to refer to the maximum as pycnocline	Feucher et al. (2016)
South Atlantic	Hydrographic CTDs and XBTs	To look for potential vorticity minimums (and then determine the thresholds of temperature gradient adapted to different mode water types)	Provost et al. (1999)
	Argo	To search for potential vorticity less than 1.50×10^{-10} m^{-1} s^{-1}	Sato and Polito (2014)
North Pacific	Argo	To look for potential vorticity less than 2.0×10^{-10} m^{-1} s^{-1}	Xu et al. (2017)
	Climatology (Ishii, EN4 and IAP data)[b]	To seek temperature gradients less than 0.015°C m^{-1}	Wu et al. (2020)
South Pacific	XBTs	To look for temperature gradients less than 0.02°C m^{-1}	Roemmich and Cornuelle (1992)
	Climatology (WOD2001) and two HRX lines[c]	To seek temperature gradient minimum	Tsubouchi et al. (2007)
Indian Ocean	Climatology (IOHB)[d]	To seek temperature gradient minimum	Tsubouchi et al. (2010)

[a]The WOD2001 represents the World Ocean Database 2001 that is a collection of objectively analyzed climatological data, and the WOCE stands for the World Ocean Circulation Experiment of which some temperature profiling data were used in this study. [b]These three datasets provide three-dimensional monthly grid temperature and salinity data (more details in Wu et al., 2020). [c]The HRX denotes the high-resolution XBT that was used to collect temperature profiles along a number of shipping transects by the Scripps Institution of Oceanography. [d]The IOHB represents the Indian Ocean HydroBase climatology.

the layer thickness greater than 100 m. In other studies, the specific thresholds of temperature or density gradient (or potential vorticity) that have been applied to define the boundaries of mode waters in certain domains remain empirical. In the next section, we will mainly compare the detecting results following the new algorithm with other studies of the South Atlantic subtropics.

2.3. Clustering Mode Waters Into Three Varieties

In previous studies, mode waters identified in the subtropical South Atlantic have been divided into three varieties. This division can be attributed to Provost et al. (1999), whose definition was based on the potential vorticity minimums found from four hydrographic CTD sections and the World Ocean Circulation Experiment (WOCE) XBT data set. This systematic study for the first time described three mode water varieties and their thermodynamic characteristics as well as thicknesses. Sato and Polito (2014) subsequently applied a k-means clustering method (Lloyd, 1982) to the more broadly distributed Argo profiles, which aimed to partition all mode water observations into a predefined number *k* of clusters (*k* = 3 in their study). This clustering analysis led to the typical classification scheme of subtropical mode waters: the one linked to the Brazil Current and its recirculation gyre (SASTMW1), the most saline variety that is directly related to the intrusion of the Indian Ocean water masses (SASTMW2), and lastly the densest one associated with the Subtropical Front (SASTMW3). Dependent on this well-established division into three mode water types, several studies (Bernardo & Sato, 2020; de Souza et al., 2018) accordingly depicted the volumetric influence of mode waters on the South Atlantic subtropical gyre circulation.

Here, following Sato and Polito (2014), a k-means clustering is applied to classify profiles that have been detected with mode waters by the new detecting algorithm into groups. Since the k-means method requires a predetermined number *k* of clusters, an evaluation follows to assess the performance of the previous clustering. All mode water profiles have been partitioned into *k* mutually exclusive clusters, such that mode waters within each cluster are as close to each other as possible, and as far from mode waters in other clusters as possible. Each cluster is characterized by its centroid and mode waters are sorted relative to the distance to this centroid with the condition that the sum of the squared Euclidean distances within each cluster is minimized. The potential temperature, salinity and potential density at the depth of median potential vorticity inside each mode water are used for each profile. These three parameters accompanied by the latitude, longitude, and season compose the six variables

that are treated equally for the classification. The variable of season corresponds to a three-month period of time (i.e., June–August is the austral winter, and so on). In addition to the division into three clusters, we also tested other possibilities, for example, $k = 2$ and 4. The $k = 2$ choice mainly separates light mode waters from dense ones, according to their potential temperature and density properties. While on the other hand, the division into four clusters further splits the SASTMW1 that originates from the western boundary into a warm variety that is presumably linked to the formation process, and a cold variety, most of which are found in the subsurface.

2.4. Co-Location Between Eddies and Argo Profiles

Satellite altimetry data provide the ideal complement to the sparse distribution of Argo profiles, which facilitate to address the issues of ocean heat and fresh water storage, transport, and variability associated with mesoscale dynamics. In the current study, we apply the eddy detection algorithm TOEddies (Laxenaire et al., 2018) that is mainly a two-step process: it first identifies eddy structures from altimetry ADT maps and then derives their trajectories together with eddy splitting and merging events. The TOEddies method also makes it possible to co-locate the detected eddies with Argo profiles that possibly capture deep mixed layers and thick mode waters. There are two types of eddy contours in the eddy detection algorithm: one is associated with the outermost closed ADT contour to define each eddy, and the other is related to the maximum azimuthal velocity of the vortex. In this study, the radius of the outer contour R_{out} is used to determine whether the location of an Argo profile falls in the scope of an eddy in that the trapped water in an eddy is not expected to stay exactly within the maximum velocity contour R_{Vmax} (Laxenaire et al., 2019). The co-location of Argo profiles and altimeter-detected eddies results in the separation of these vertical profiles into three groups: those sampling a cyclonic eddy, those sampling an anticyclonic eddy, and those falling outside of either type.

Sometimes these eddies evolve in the ocean interior along their trajectories, but their signatures often remain measurable at the surface so that they can still be detected by satellites. Next, a method that separates subsurface-intensified eddies from surface ones is introduced to partition these altimeter-detected eddies and associate the eddy vertical locations with mode water detection. This separation is accomplished by taking into account the pressure-dependent SHA, h', following the definition by Gill and Niller (1973):

$$h'(p) = \frac{1}{\rho_0} \int_{1500}^{p} \sigma_0' dp, \tag{3}$$

where ρ_0 is the reference seawater density and σ_0' is the anomaly of potential density, relative to a climatological profile that represents the local environment. The pressure of 1500 dbar is regarded as the no-motion reference level. For each profile detected with an eddy from the TOEddies algorithm, its related climatological profile is calculated as an average over all profiles that satisfy both criteria of locations and time. Spatially, these profiles are supposed to be positioned within a rectangular box of $2.5° \times 2.5°$ centering on the eddy profile, while the selection based on time applies a window spanning over 30 calendar days (i.e., independent of the year) from the date of the eddy. These criteria ensure that the anomaly profile σ_0' is restricted to local variations.

For each eddy, the h' displays a different shape of profile. Those with larger h' values in the subsurface compared to the surface could be representatives of subsurface-intensified eddies. Alternatively, h' maximum is usually found within surface layers for profiles presumably representing surface-intensified eddies. In this study, the previously detected MLD is used as the depth criterion for classifying an eddy as surface or subsurface. That is, subsurface eddies are defined by h' profiles with maximum values below the MLD. The sign of h' also determines the polarity of an eddy: cyclonic eddies are correlated with negative h', while the profiles displaying positive values of h' are associated with anticyclonic eddies.

It is also of interest to test whether this SHA separation of surface and subsurface eddies could be applied alone as eddy detecting method (i.e., without any detection derived from altimetry maps at the beginning). Though sometimes subsurface eddies are observed to exert sea surface signatures and thus can be detected from satellites, the proportion remains unclear. However, an obvious issue with the SHA method is that almost every SHA profile predetermines an eddy since the profile typically holds an h' maximum no matter at what depth it is located. Thus, some discussions regarding the possibility of eddy detection by SHA are provided in Appendix A.

Table 2
The Domain-Averaged Mixed Layer Depths (MLDs) and Their Associated Standard Deviations for Three 10° × 10° Regions Shown in Figure 4a

	Threshold MLD (a)	Gradient MLD (b)	Hybrid MLD (c)	Curvature MLD (d)
Box 1	63.8 ± 57.6	44.6 ± 48.2	62.8 ± 52.7	60.5 ± 58.7
Box 2	54.3 ± 39.8	35.5 ± 31.5	57.4 ± 40.6	52.9 ± 42.8
Box 3	71.6 ± 60.6	53.6 ± 57.0	67.0 ± 57.3	67.7 ± 60.4

Note. A detailed profiling picture is also provided in Appendix B. Unit: m. Here, the mean MLD for each method was calculated for all profiles inside each box (i.e., no limitations on time).

3. Results

3.1. Comparison of MLD Detections

Figure 4 compares four MLD detecting methods that are based on the density profiles. The upper panels show more traditional approaches defined by (a) a density threshold of 0.03 kg m^{-3} (de Boyer Montégut et al., 2004) and (b) a density gradient threshold of 5×10^{-4} kg m^{-4} (Dong et al., 2008). The lower panels show the comparison between (c) a more complex hybrid detection based on density (Holte & Talley, 2009) and (d) the method we have developed that relies on gradients and curvatures. These maps were calculated by averaging the five deepest values found from all Argo profiles that fall in each 1° × 1° grid. Therefore, Figure 4 preferentially depicts the mixed layer patterns in winter that might be helpful to compare with locations of outcropping mode waters afterward. In general, the resulting MLD of an application of density gradient threshold in (b) stands out as the shallowest estimate compared with the other three methods.

In the thermodynamically cooling regions, poleward of 35°S, the magnitude of curvature-derived MLD of (d) is in the middle of a larger threshold-based estimate of (a), and a slightly smaller value of (c) by the hybrid method. Specifically, the spatial pattern of (a) displays very similar results to (d), though the threshold method in theory can hardly capture any small vertical gradients and thus might overestimate the MLD. In fact, of the total number of profiles (122,202), 96,650 profiles (79.1%) were detected by the density threshold and the new methods with the same MLD value. This similarity further draws attention to the necessity of density threshold as a validation factor in the new algorithm. In the subtropical regions (equatorward of 35°S), where the seasonal cycle of stratification is typically weaker than its diurnal cycle, the vertical gradients remain mostly unchanged from the surface down to the top of the pycnocline. As a result, the MLD detection by local extremes of curvature, as shown in (d), can precisely trace the depth at which the gradient greatly changes and the curvature stands out.

To further present the differences among these four MLD detection methods, three squared domains were selected (shown in Figure 4a) and for each domain we thus calculate the mean MLD values and their associated standard deviations for each detecting method. The result is also displayed in Table 2. It is consistent with the spatial distribution of maximum MLDs in Figure 4 that the gradient-dependent method (b) always leads to the shallowest MLD compared with the other three methods. Though the curvature-based MLD value is either closer to the MLD resulted from the single density threshold or roughly the same as the hybrid MLD, the standard deviation of this curvature-derived MLD always remains the largest among the four methods. At the same time, the gradient method (b) produces the smallest standard deviations compared with others. This suggests that the curvature method might be more capable of taking into account the spatial variability of MLDs for all profiles in one specific domain, which further implies that this approach is better at capturing small gradient changes for different profiles. However, it requires further studies to compare the precision of these four MLD detecting methods and to determine which method better represents the surface ocean state after mixing.

3.2. General Characteristics of the SASTMW

Before the general description of SASTMW, Figure 5 shows the patterns of SST, sea surface salinity (SSS), heat flux, and eddy kinetic energy (EKE) in the South Atlantic Ocean over months from July to October (austral winter). The SST and SSS patterns are displayed to provide the location of the Subtropical Front along 40°S that separates the subtropical domain from the subantarctic region, which is indicative of the boundary of SASTMW. These maps are also overlapped with the season-averaged ADT contours in dark gray and bottom topography in light brown, respectively showing the upper-ocean general circulation and providing positions where mode waters might be formed and transported.

Figure 5c then displays the pattern of winter cumulative heat flux to estimate the strength of winter cooling. Regions of heat loss excess would be regarded as favorable areas of mode water formation or renewal due to the commonly observed co-occurrence with convective mixing maximum. In the subtropical South Atlantic, it seems obvious that two regions dominate as venues of intense heat loss to the atmosphere. The western region is located
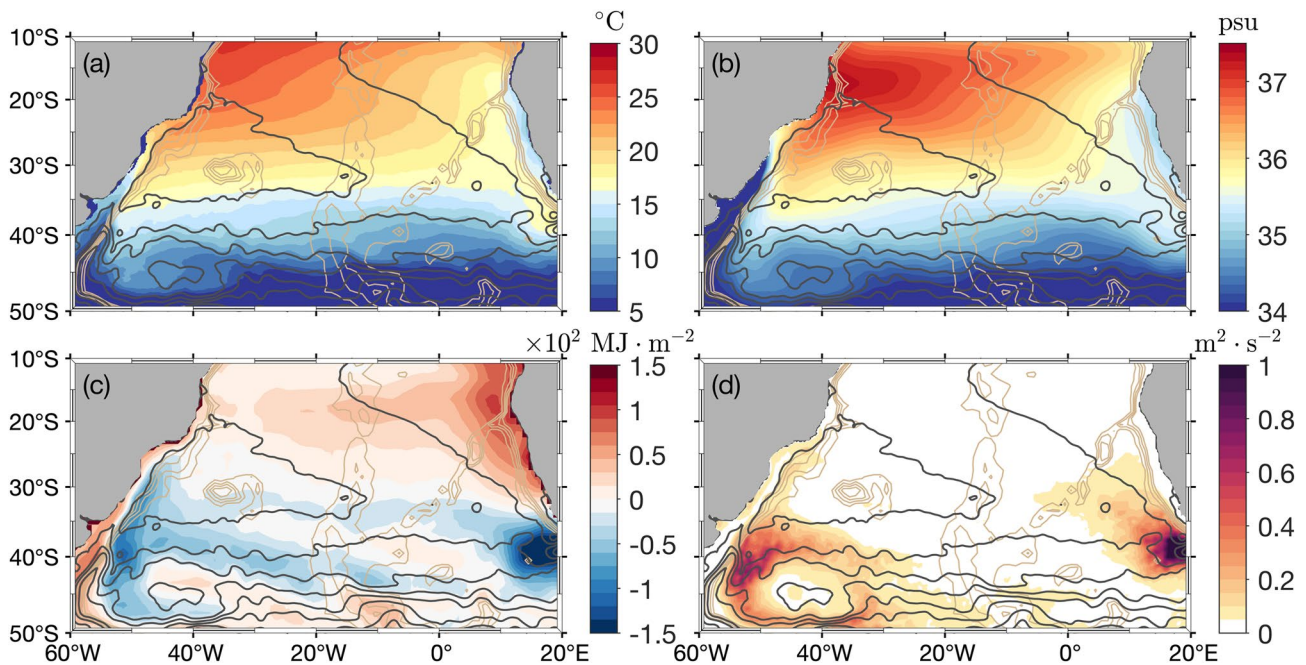
Figure 5. Spatial patterns of austral winter-time (a) mean sea surface temperature (SST) calculated over daily maps of the period 2000–2016 from the European Space Agency (ESA) Climate Change Initiative (CCI) database (Merchant et al., 2019), (b) mean sea surface salinity (SSS) averaged over the monthly database from 2000 to 2018 archived in the Copernicus Marine Service (Droghei et al., 2018), (c) cumulative heat flux (positive downward) calculated by adding the daily maps between 2002 and 2009 from the WHOI OAFlux Project (Yu et al., 2008), and (d) cumulative eddy kinetic energy (EKE) in the South Atlantic region, derived from the SLA field and based on the geostrophic relationship (Pujol et al., 2016). The austral winter in these maps is defined from July to October. The overlapping dark gray lines indicate the season-averaged ADT contours (provided by SSALTO/Data Unification and Altimeter Combination System [DUACS]) and the light brown lines show contours of bathymetry over – 3,600 to –1,800 m.

at the confluence zone where the Brazil Current meets the Malvinas Current (Gordon, 1989), while the eastern region corresponds to the dynamics of Agulhas Rings in the southeastern Cape Basin, stimulated by the intrusion and retroflection of the Agulhas Current that brings warm and salty waters from the Indian Ocean (Capuano et al., 2018; Gordon et al., 1992; Speich et al., 2007). Those regions with intense cooling are also consistent with the EKE pattern shown in (d), suggesting a possible role of mesoscale dynamics in buoyancy loss, mode water formation, and transport.

3.2.1. Outcropping and Subsurface Mode Waters

Counting both outcropping and subsurface components in the subtropical South Atlantic, in total, we detected SASTMWs in 10,472 profiles (with 7,375 outcropping mode waters, and 3,097 subsurface mode waters that also involve 50 profiles with double cores at depth). When limited to the south of 15°S and north of 45°S, some profiles are intentionally excluded. That is, the total number of 10,472 profiles was confined to this latitudinal band, while other mode waters exist outside this domain yet still fill in the ranges of temperature, salinity, and density of subtropical mode waters in the South Atlantic. This process of exclusion is added because the temperature and salinity of mode waters in the South Atlantic show a wider spectrum especially compared with, for example, the 18° Water as one type of the North Atlantic subtropical mode waters. A specific constraint of latitudes and longitudes is thus required to separate the subtropical mode waters from subantarctic ones in the South Atlantic. For example, outcropping mode waters located within the Zapiola basin might be one type of Subantarctic Mode Water (SAMW) formed on the northern flank of the Antarctic Circumpolar Current (Herraiz-Borreguero & Rintoul, 2011). From this perspective, we set the southern boundary of 45°S to exclude other water masses.

Figure 6 illustrates the maximal values of mode water thickness calculated by the new algorithm and displays two configurations in terms of the vertical. To spatially interpolate the scatter pattern of mode waters to show a more general distribution, the maximal values of mode water thickness were selected in each 1° × 1° grid and those isolated mode water dots that are not connected to other profiles were removed. For this reason, the spatial patterns of both (a) outcropping and (b) subsurface mode waters display thoroughly connected belts. The upper
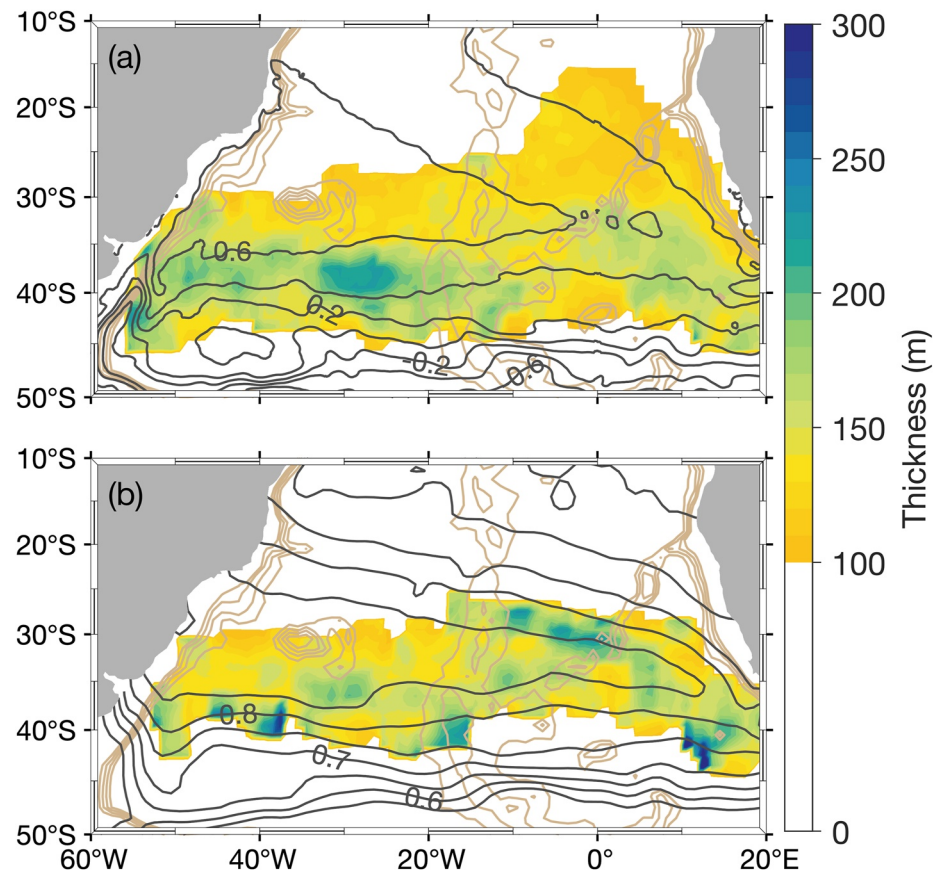
Figure 6. Maximal mode water thicknesses for (a) outcropping mode waters overlapped by the mean dynamic topography (MDT) as contours in dark gray (Mulet et al., 2021); and (b) subsurface mode waters instead superimposed by the steric height (anomaly) contours at 400 dbar integrated from 1200 dbar and averaged in each $1° × 1°$ grid (Boyer et al., 2019). If more than one subsurface mode water is detected for a profile, the thickness is the sum of the two subsurface mode waters. The light brown contours draw the mean pattern of bottom topography over −3,600 to −1,800 m.

panel shows a thick outcropping mode water layer developed in the southwestern part of the subtropical gyre where warmer water carried by the southward Brazil Current is subject to severe winter cooling by the polar air outbreaks from the continents, and as it encounters the Malvinas Current that brings cold water northward. The thickest outcropping SASTMWs are found at the eastern boundary of the Brazil Current recirculation gyre nearby 30°W. More generally, thick layers of outcropping mode waters extend along the South Atlantic Current from the Brazil-Malvinas Confluence region as well as along the path of Agulhas Rings in the Cape Basin, at the eastern end of the subtropical gyre.

The distribution of subsurface SASTMW thickness is displayed in Figure 6b. Superimposed are the steric height contours at 400 dbar that result from an integration over all climatological profiles starting from 1,200 dbar. Such contours illustrate the subsurface structure of the ocean circulation and, in particular, that of the subtropical gyre which shifts poleward at depth. The figure shows that the subsurface SASTMW is confined within and spans across the entire subtropical gyre. Analogous to the pattern of outcropping mode water thickness, the thickest layers are also located along the South Atlantic Current with maximums situated on top of the Mid-Atlantic Ridge and nearby 40°W. Other regions of relatively thick subsurface mode waters are observed along the routes of Agulhas Rings in the eastern and northern areas of the subtropical gyre. Agulhas Rings carry transformed Indian warm and saline waters northwestward, following the subsurface Benguela Current system (Guerra et al., 2018; Laxenaire et al., 2019), with the thickest subsurface mode waters situated between the Walvis and Mid-Atlantic Ridges.
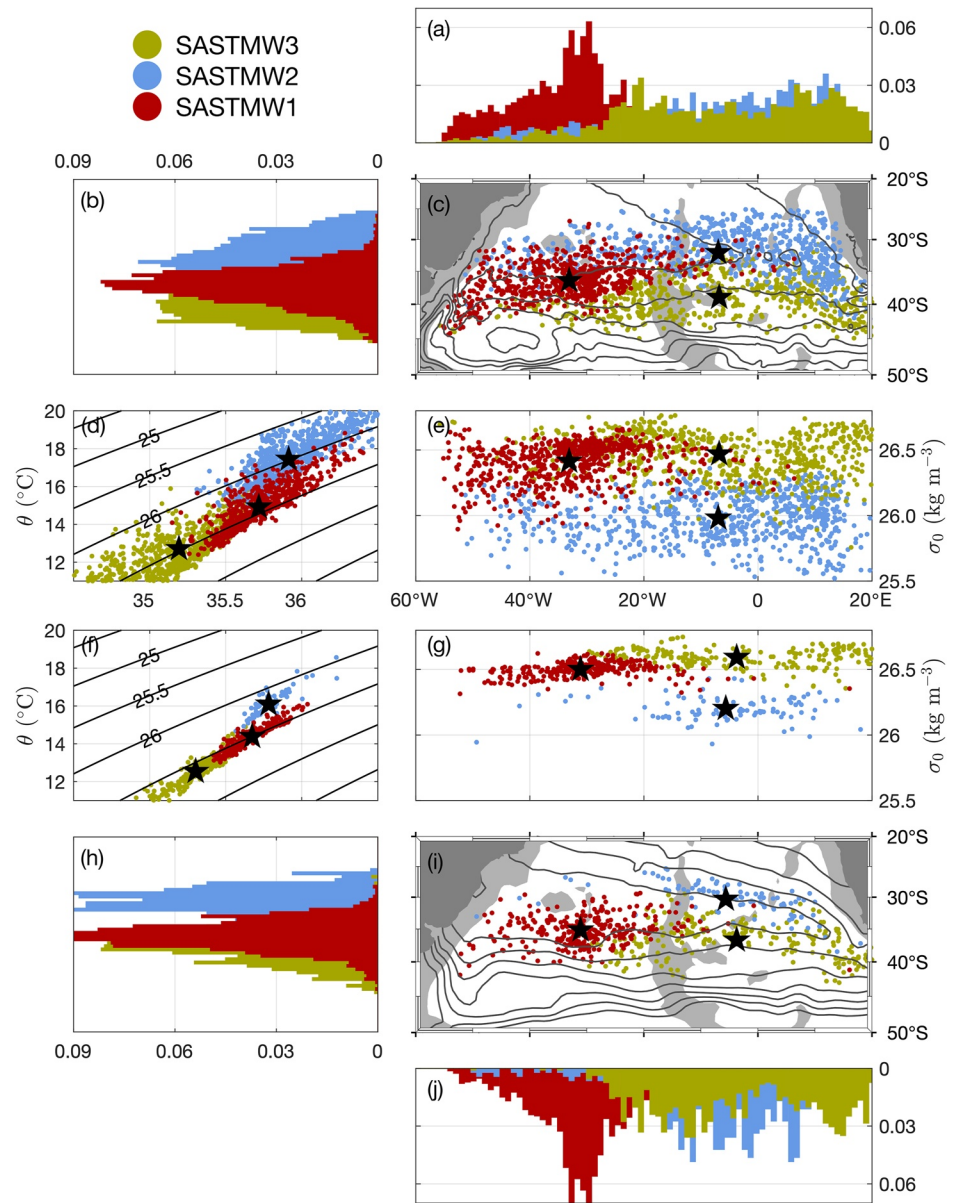
Figure 7. Three types of SASTMW selected by the cluster analysis based on parameters measured at the depth of median potential vorticity of each mode water layer: SASTMW1 (red), SASTMW2 (blue), and SASTMW3 (green). The upper five panels (a–e) provide an analysis of the total number of mode water layers and the lower five panels (f–j) comparatively show another analysis only for subsurface mode waters. These panels contain (a/j) histograms as a function of longitude; (b/h) histograms as a function of latitude; (c/i) the spatial distributions; (d/f) temperature-salinity diagrams with potential density contours; and (e/g) the potential density as a function of longitude. The location of centroids determined by the cluster analysis is identified as black stars. For the two patterns of spatial distribution, (c) is overlapped with the mean dynamic topography (MDT) as contours (Mulet et al., 2021), while (i) is superimposed by the steric height (anomaly) contours at 400 dbar integrated from 1,200 dbar.

3.2.2. Cluster Analysis of the SASTMW

A cluster analysis is applied to separate the SASTMW profiles based on six parameters that bind similar members together. The difference between our analysis and that of Sato and Polito (2014) is that in our method the parameters were picked at the depth where the median potential vorticity was found within the detected mode water layers while their target depth of the median potential vorticity was spotted from the entire profile. At first sight of Figures 7a–7c, the separation leads to three clusters with their centroids respectively located in the

west (SASTMW1), northeast (SASTMW2), and southeast poleward edge of the subtropical gyre (SASTMW3). Generally, mode waters in the SASTMW1 cluster are concentrated around the Brazil Current extension and its recirculation area, situated in the western side of the basin. Figures 7d and 7e show that SASTMW1 is characterized by intermediate values of properties between SASTMW2 (the warmest, saltiest, and lightest variety) and SASTMW3 (the coldest, freshest, and densest of the three). In favor of comparison, the colors of these three varieties were intentionally chosen to match the separation in Figure 4 of Sato and Polito (2014). Consistent with the general separation patterns of both Sato and Polito (2014) and Provost et al. (1999), Figure 7 also brings several detailed differences. Concerning the separation between SASTMW1 and SASTMW2, it is evident from (d) the T-S diagram that SASTMW2 contains mode waters with more saline properties than SASTMW1. However, such is not the case in the study of Sato and Polito (2014), of which the two varieties of mode waters share the same salinity range. The overlapped area of any pairwise combination remains large, while these three varieties are more separable in Sato and Polito (2014).

Besides the general division of SASTMW into three clusters, Figure 7 also displays a separation of mode waters by configuration. The lower five panels (f-j) provide another cluster analysis limited to only subsurface mode waters. In comparison to a broader range of the potential density of total mode waters, the three varieties of subsurface mode waters are characterized by densities above 26 kg m^{-3}, with shrinking density range in each cluster. Noticeably, both subsurface SASTMW2 and SASTMW3 shift northward in contrast to the total SASTMW2 and SASTMW3 patterns (focusing on the comparison of histograms [b] and [h]). The spatial distribution of subsurface SASTMW2 in (i) approximately follows the route of subduction along the deep Benguela Current. This shift also implies that the SASTMW3 stems more likely from the water supply shedding from the Agulhas Current into the Cape Basin that contains Indian warm and saline properties. Sato and Polito (2014), on the contrary, attribute the origin of SASTMW3 derived from their calculation to the western boundary that can be transported by the South Atlantic Current along the southernmost boundary of the subtropical gyre toward the east. In other words, they suggested the same formation region for SASTMW1 and SASTMW3 in that both have footprints west of 45°W and south of 40°S. However, it is thus difficult to explain the mechanisms that separate these two mode water types holding similar density ranges.

With the aim to specify the genesis and evolution of individual mode water types, Figure 8 then highlights the information of layer thicknesses divided into outcropping and subsurface ones. The outcropping SASTMW1 variety (Figure 8a, holding 1,782 profiles and taking up 17.0% of the total number) concentrates in the south-westernmost part of the subtropical gyre between the Confluence region and the Subtropical Front mostly west of the Mid-Atlantic Ridge. The subsurface SASTMW1 (Figure 8b, counted in 1,712 profiles in total [16.3%]) is extensively distributed across the inner core of the deep subtropical gyre. While the averaged thickness of outcropping SASTMW1 reaches 164 m, the mean thickness of subsurface SASTMW1 is slightly lower (142 m). Composed of 3,378 profiles in total (32.3%), the outcropping SASTMW2 (Figure 8c) spans over the north-eastern portion of the subtropical gyre and reaches the far west coast. The SASTMW2 in the subsurface (Figure 8d, with 395 profiles [3.8%]) outspreads the northeastern part of the basin, displaying an explicit path of thick mode water layer along the deep Benguela Current. The spatial distribution of total SASTMW2 and its length of spreading thus imply that the Benguela Current and potential paths of Agulhas Rings play a crucial role in advecting mode waters zonally to the west (Stramma & England, 1999). The mean thicknesses of outcropping and subsurface SASTMW2 reach 133 and 147 m, respectively, and this is the only type of the three featured by a much thicker subsurface mode water layer than the outcropping one. The SASTMW3 that outcrops (Figure 8e, displaying 2,215 profiles [21.2%]) lies in the south-easternmost part of the gyre, with the thickest water layers clustering along the South Atlantic Current above the Mid-Atlantic Ridge as well as aligned along the routes for Agulhas Rings. Although the thickest layers of outcropping SASTMW2 and SASTMW3 approximately overlap at the intrusion of Agulhas Rings, it is plausible to associate the SASTMW2, the lighter SASTMW variety, with the northern and central routes of Agulhas Rings and to relate the SASTMW3, the denser variety, to the southern route as described in Dencausse et al. (2010). It is also the case for the comparison between these two varieties in the subsurface that SASTMW3 (Figure 8f, with 990 profiles [9.5%]) penetrates in the subtropical gyre from the Cape Basin and extends until the Mid-Atlantic Ridge, following a route more southern and deeper than that of the subsurface SASTMW2. The averaged thickness of outcropping SASTMW3 is 150 m, and this value is similar to the subsurface SASTMW3 thickness, which reaches 151 m. In general, our calculation results in thinner mode waters compared with Sato and Polito (2014); however, both studies suggest that SASTMW2 is characterized as the thinnest type of the three.
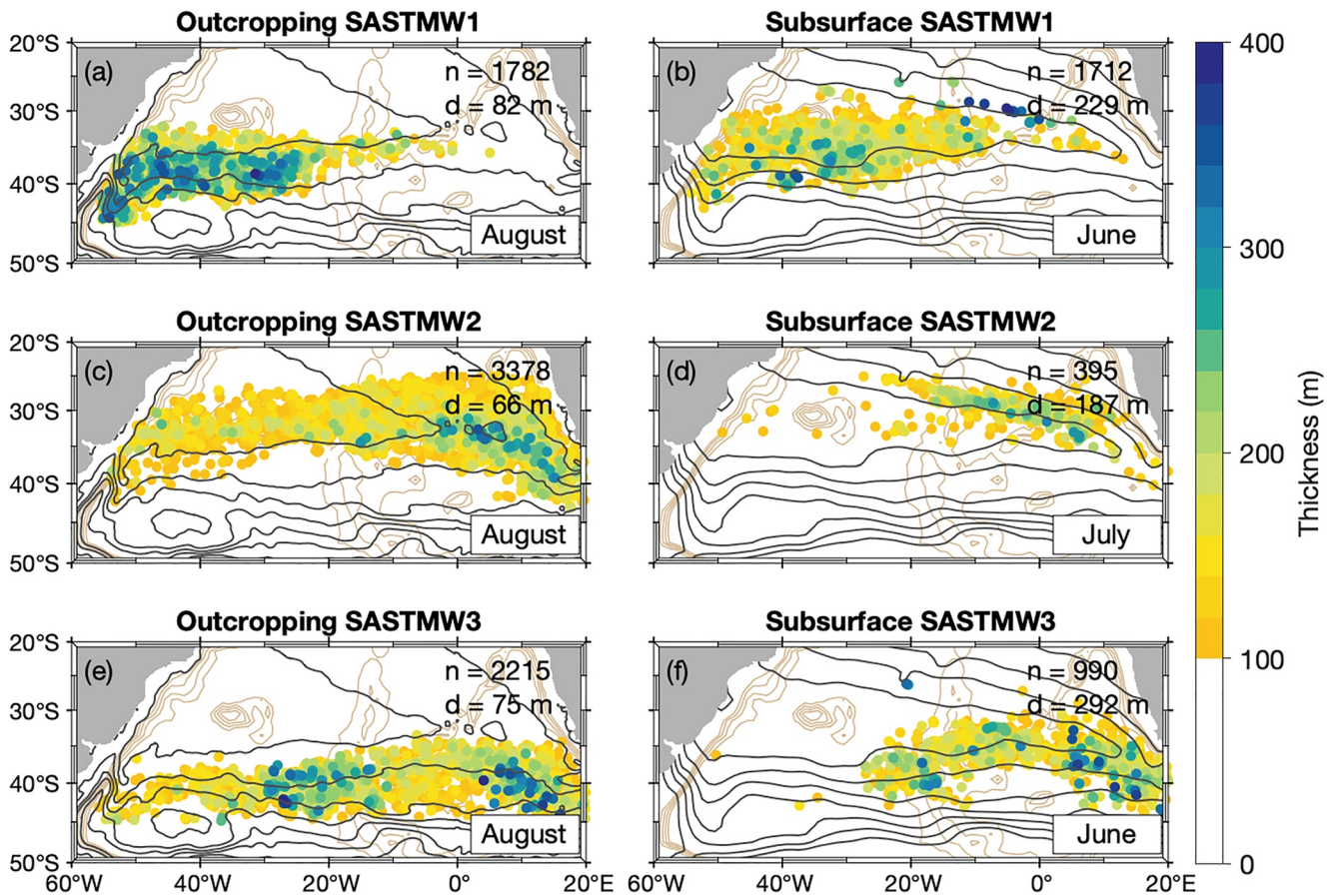
Figure 8. The thicknesses of outcropping and subsurface mode waters. The number *n* on the top right corner of each panel indicates the number of profiles detected as mode waters for each specific type. The number *d* is indicative of the mean depth of mode waters. Panels of outcropping mode waters (a), (c), and (e) are overlapped by the mean dynamic topography (MDT) as contours in dark gray (Mulet et al., 2021) and panels of subsurface mode waters (b), (d), and (f) are superimposed by the steric height (anomaly) contours at 400 dbar integrated from 1,200 dbar. The light brown contours draw the mean pattern of bottom topography over −3,600 to −1,800 m. At the bottom right corner in each panel, the averaged month of occurrence for mode waters is added.

As expected, the outcropping SASTMW layers are found mostly in winter and early spring months in coherence with the formation processes whereas the subsurface varieties are identified at any time, suggesting that these waters move in the ocean interior and are disconnected from any interaction with the atmosphere. This is true in Figure 8 that the averaged month of occurrence for outcropping mode water detection is concentrated in July and August (austral winter), while the subsurface mode waters could be found at any season of the year (not shown). This seasonal variation, together with their spatial distribution, suggests that SASTMW1 is formed at the southwestern edge of the subtropical gyre. Once subducted, these mode waters move in the gyre interior following the recirculation flow. By contrast, the SASTMW2 and SASTMW3 both take their origins mostly in the eastern corner of the subtropical gyre in the Cape Basin and extend toward the western boundary.

As mentioned earlier, a similar cluster analysis by Sato and Polito (2014) assigned the formation and transport of SASTMW3 to the Subtropical Front of the South Atlantic Current, suggesting that any potential subduction processes of mode waters are linked to the eastward transport. Other differences between our cluster analysis and theirs are also observed. For example, we have detected more subtropical mode water layers compared with them (also taking into account 5 more years of profiles). A more recent revisit to the cluster analysis of SASTMW (Bernardo & Sato, 2020) confirms that even using a more restricted temperature range to select subtropical mode waters, it still yields a division into three clusters that highly matches the results of Sato and Polito (2014). In both studies, the spatial distribution of each mode water type is almost entirely separated from others, while in our study different varieties overlap in their properties (compare Figure 8 with Figure 5 in Sato & Polito, 2014). Another evident difference between our results and those of Sato and Polito (2014) is related to the thickness
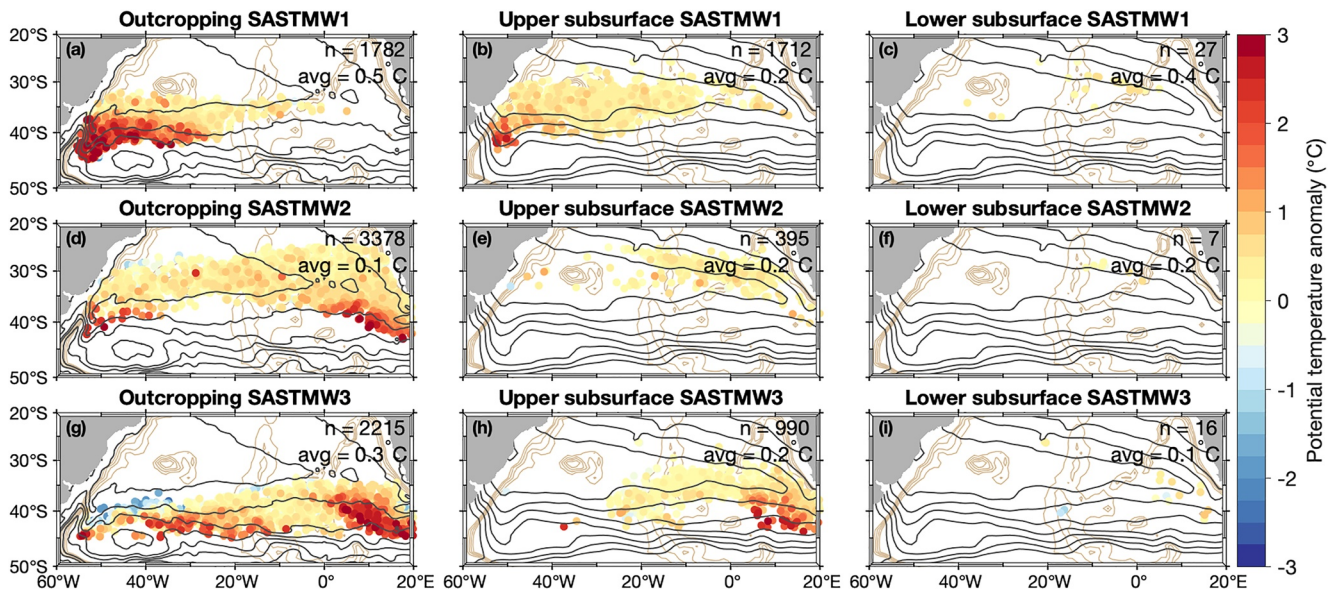
Figure 9. The potential temperature anomaly of outcropping and subsurface mode waters. These values of anomaly were calculated as the difference between the original Argo profiles and climatological profiles associated with each individual Argo profile (Laxenaire et al., 2019). The number *n* on the top right corner of each panel indicates the number of profiles detected as mode waters, and the value marked by *avg* is the mean value of potential temperature anomalies averaged over all mode waters. Panels of outcropping mode waters are overlapped by the mean dynamic topography (MDT) as contours in dark gray (Mulet et al., 2021), and panels of subsurface mode waters are superimposed by the steric height (anomaly) contours at 400 dbar integrated from 1200 dbar.

pattern. Both studies display similar hotspot areas of thickest mode waters, but Figure 8 provides a more obvious route of mode water transport along the paths of Agulhas Rings.

3.2.3. Temperature Anomalies of Mode Waters

Laxenaire et al. (2019) suggested that heat content anomalies transported by Agulhas Rings were concentrated in mode water cores. Here, we quantify the potential temperature anomalies calculated within each mode water layer, which helps to understand the amount of heat anomalies carried by mode waters. Figure 9 displays the anomaly for the three types of SASTMW and further shows a division of subsurface mode waters into upper (middle panels) and lower cores if present (right panels). The anomaly is computed as the subtraction of the climatological temperature from each Argo profile and averaged over isopycnals of mode water layer to obtain a single value for each detection. The pressure coordinate is commonly used to calculate the anomaly within mode water layers (e.g., to integrate anomalies over pressure or depth); nonetheless, the computation in Figure 9 is based on the density coordinate and this choice more correctly captures the anomaly values, which highlights the different abilities of mode waters and the environment in trapping heat. It is also interesting to note the existence of lower subsurface mode water cores in some profiles (albeit much fewer in number than the upper subsurface and outcropping ones, only counted in 50 profiles). In other words, the double-core profiles that are more or less indicative of co-location between water masses with different origins, are sparse and mostly limited to the Brazil Current recirculation gyre or narrowed within the routes of Agulhas Rings.

The regions of Brazil-Malvinas Confluence and paths of Agulhas Rings constitute the two main areas of heat release to the atmosphere, and hence favorable for convective mixing and water mass formation. Counter-intuitively, all panels in Figure 9 display warm temperature anomalies inside mode water layers as compared to the monthly averaged environment. The maximal warm anomalies of outcropping SASTMW1 shown in Figure 9a are situated exactly at the Brazil-Malvinas Confluence zone and extend along the Subtropical Front. This mode water type originates from the southward Brazil Current that carries tropical warm and saline waters. It is also evident in Figures 5a and 5b that local hotspots of SST and SSS exhibit at the western boundary with centers at 15°S and 18°S, respectively. The other two types of mode waters, SASTMW2 and SASTMW3, initiate from the Agulhas Leakage where Indian warm and saline waters overshoot via anticyclonic Agulhas Rings. Interestingly, the spatial pattern of temperature anomalies inside SASTMW2 and SASTMW3 is also consistent with studies of individual Agulhas Ring tracking that correspond the salt and temperature fluxes over the Agulhas Leakage to
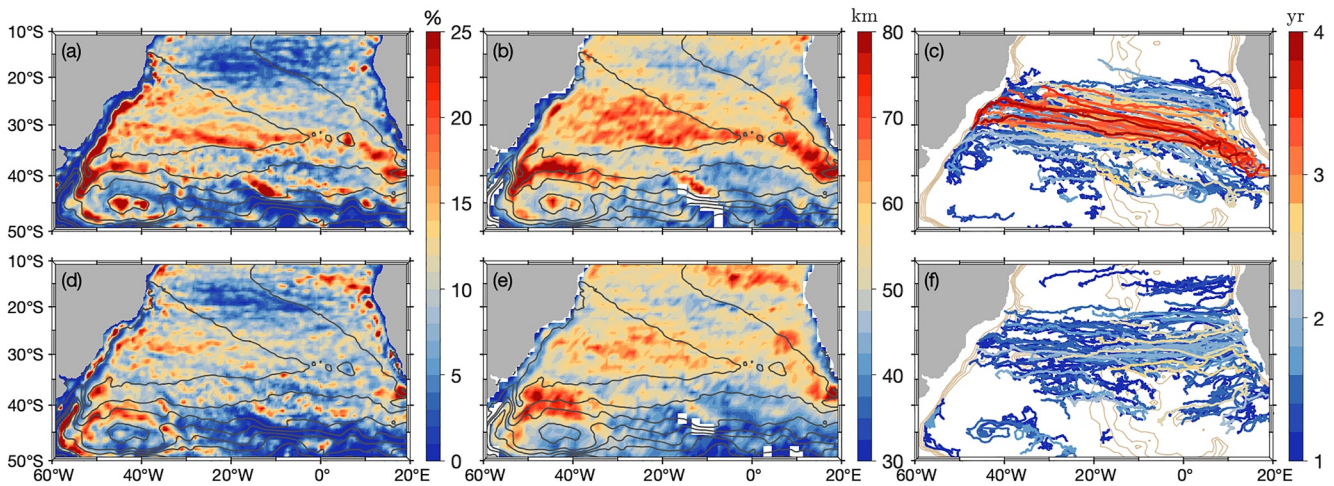
Figure 10. The characteristics of mesoscale eddies in the South Atlantic detected from the TOEddies algorithm (Laxenaire et al., 2018). The panels show (a/d) the presence indicated by percentage, (b/e) radii, and (c/f) trajectories along with their lifetimes of anticyclonic eddies (in the upper panels) and cyclonic eddies (in the lower panels). The gray contours indicate the mean dynamic topography (MDT) as an estimate of the mean sea surface height above geoid over the 1993–2012 period (Mulet et al., 2021). The light brown lines at the background in (c) and (f) show contours of bathymetry over –3,600 to –1,800 m.

these rings more than their surroundings (Laxenaire et al., 2019). These facts recall a possible link between mode water transport and mesoscale eddies, with an emphasis on the anticyclonic ones that can trap such anomalies inside isopycnal layers. In the next section, we specifically focus on such analysis.

3.3. Co-Location of SASTMW With Mesoscale Eddies

Here, a specific focus on the connection between mesoscale eddies and mode waters is studied. Mesoscale eddies are detected by the TOEddies algorithm from altimetry ADT maps (Laxenaire et al., 2018). Figure 10 displays (a/d) the presence of anticyclones/cyclones in percentage of time at each altimetric grid point, (b/e) their maximum radii in each $1° \times 1°$ grid cell and (c/f) trajectories of anticyclonic/cyclonic eddies living more than 1 year in the South Atlantic. These maps show that eddies are particularly present near the basin boundaries, but also located across the South Atlantic where they cluster along quasi-zonal paths, with the longer-lived eddies propagating from the eastern boundary westward. The adjacent area of the Brazil Current and its interaction with the Malvinas and South Atlantic Currents are occupied by both cyclonic and anticyclonic eddies, with more intense presence and larger size of anticyclones. The Zapiola gyre appears as a very active region for both eddy polarities. The presence of cyclonic eddies specifically follows the Benguela Current along the eastern coast while the anticyclonic eddies are largely linked to the formation of Agulhas Rings and their transport westward in a zonal band centered at around 35°S. It is more apparent from the trajectories of anticyclonic eddies that under certain circumstances, these eddies can live for more than 3 years and travel across the entire basin (Laxenaire et al., 2018).

Of the total number of Argo profiles (122,202) in the South Atlantic as shown in Figure 1, 15,093 (12.4%) and 15,945 (13.0%) profiles are respectively co-located with TOEddies cyclonic and anticyclonic eddies. This result is consistent with a statement in Sato and Polito (2014) that Argo profilers indicate indifference to the presence of mesoscale eddies. In their study, 19.6% of Argo profiles were observed inside eddies identified and cataloged by Chelton et al. (2011). Here, mode waters are more likely to be found in an eddy (41.6% out of the total mode water number of 10,472). This fraction is largely enhanced compared with the proportion of profiles that generally sample eddies. However, Sato and Polito (2014) showed that mesoscale eddies co-located with mode waters display a similar percentage (22.4%) to that of the general co-location between eddies and all profiles.

A more detailed co-location between mesoscale eddies and mode waters is shown in Figure 11. The left panels (a), (c), and (e) compare the presence of outcropping SASTMWs falling within anticyclones, cyclones, and outside of eddies, while the right panels (b), (d), and (f) show the relationship between subsurface mode waters and eddies. In general, mode water layers co-located with anticyclonic eddies are thicker and more expansive than those inside cyclones. This difference is particularly evident for the subsurface SASTMW, for which the co-located anticyclones outnumber cyclones by 4 to 1. It is also of interest to compare the region of maximum thickness
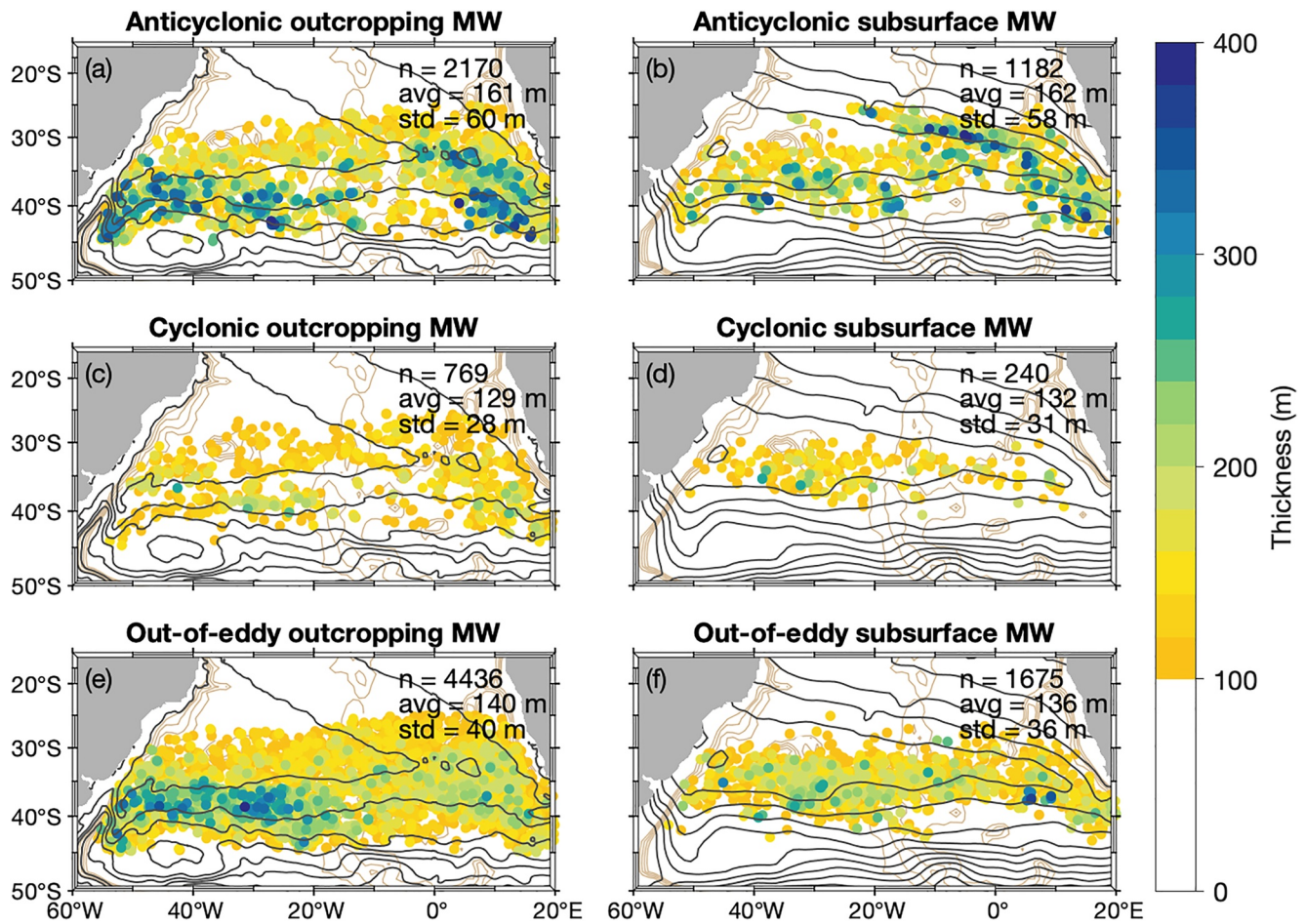
Figure 11. The co-location between mode waters and mesoscale eddies detected by TOEddies algorithm. Left panels show outcropping mode waters associated with (a) anticyclones, (c) cyclones, and (e) neither type. Right panels (b), (d), and (f) display the co-location between subsurface mode waters and eddies. The numbers marked by *n*, *avg*, and *std* are respectively indicative of the total number, mean value, and standard deviation of mode water thicknesses. The gray contours in the left panels indicate the mean dynamic topography (MDT) as an estimate of the mean sea surface height above geoid over the 1993–2012 period (Mulet et al., 2021), whereas in the right panels they represent the steric height (anomaly) contours at 400 dbar integrated from 1,200 dbar and averaged in each 1° × 1° grid. The light brown contours show bathymetry over −3,600 to −1,800 m.

in Figures 11a with the left panels in Figure 9 of temperature anomalies. This comparison strongly supports that positive temperature anomalies are associated with anticyclones. The presence of subsurface SASTMWs inside anticyclones (Figures 11b) also suggests a route of water subduction following the paths of westward Agulhas Rings, with the thickest mode water layers lying between the Malvis Ridge and Mid-Atlantic Ridge. Though the number of mode waters trapped inside eddies remains smaller than those falling outside, it is still obvious that the thickest mode waters are commonly inside anticyclones. Additionally, both out-of-eddy outcropping and subsurface mode waters (Figures 11e and 11f) show similar patterns to co-location between mode waters and anticyclones (Figures 11a and 11b), but with relatively smaller thicknesses. It is worthwhile recalling that in the TOEddies algorithm, only those subsurface-intensified eddies that still maintain a surface signature are detected. In this regard, it is very likely that some subsurface eddies are not strong or stable enough to be detected by altimetry maps, but they are still efficient in transporting mode waters. In Appendix A, we further discuss this perspective in details of whether the SHA can be regarded as an alternative to the TOEddies or other altimetry-derived eddy detecting methods, in order to detect eddies simply from Argo profiles.

To complete the SASTMW-eddy analysis, we apply an eddy separation process based on the calculation of SHA for each Argo profile that is co-located with an eddy, in favor of dividing eddies into surface-intensified and subsurface-intensified types. Table 3 displays such division by showing the percentage of mode waters trapped in eddies. The calculation of percentage was separated by the two mode water configurations (i.e., the sum of

Table 3
The Percentage of Mesoscale Eddies Associated With Mode Water Detection

	Outcropping mode water		Subsurface mode water	
Anticyclonic TOEddies	29.4		38.2	
(Surface/subsurface)	21.8	4.3	11.9	23.1
Cyclonic TOEddies	10.4		7.7	
(Surface/subsurface)	2.6	6.0	1.6	4.8
Outside of TOEddies	60.2		54.1	

Note. The percentage was calculated relative to the numbers of outcropping and subsurface mode waters, respectively.

outcropping mode waters is 100%, and so is the sum of subsurface mode waters). It is evident for both outcropping and subsurface mode waters that anticyclonic eddies trap three and five times more of the quantity than cyclonic eddies, respectively, even though the largest quantity of mode waters drop outside of either type. This is also in accordance with several previous studies that anticyclones provide favorable conditions for mode water formation and transport (Sato & Polito, 2014; Uehara et al., 2003). Moreover, it is also true that the SHA method does not always provide a division into surface-intensified and subsurface-intensified eddies. This is due to several factors such as insufficient length of profiles, unidentified peaks of the SHA profiles, and so on. Unsurprisingly, surface anticyclones play a crucial role in transporting outcropping mode waters while subsurface mode waters are more likely to be co-located with subsurface anticyclones. However, this is not the case for cyclonic eddies, which show preferences toward subsurface ones to trap both outcropping and subsurface mode waters. Since the separation of surface-intensified and subsurface-intensified eddies depends on the MLD, the relatively shallow mixed layers associated with cyclonic eddies allow more eddies to be detected as subsurface eddies.

4. Discussion and Conclusion

A simple algorithm to estimate the upper ocean mixed layers and mode waters has been presented, which is dependent on the gradients and curvatures of each individual Argo profile. In comparison with previous MLD detecting methods according to (temperature or density) thresholds and gradient thresholds, this new algorithm determines the base of the mixed layer in a more explicit way that accurately locates the depth at which the gradient greatly changes. This algorithm is specifically applied to the subtropical South Atlantic and helps to gain new insights into mode water formation and transport associated with several mechanisms, for example, air-sea heat exchanges, western boundary current system, and water intrusion from another basin.

In particular, we revisit the cluster analysis of Sato and Polito (2014) to divide all SASTMWs into three varieties, yet the division leads to different results. The major difference is associated with the origin of SASTMW3, the densest variety of these three mode water types. We observe that both SASTMW2 and SASTMW3 develop essentially in the southeastern Cape Basin where the warm Agulhas Current leaks water via the Agulhas Retroflection and forms Agulhas Rings. Only a small fraction of SASTMW3 seems to originate from the South Atlantic Current before its interception by the Mid-Atlantic Ridge. Conversely, Sato and Polito (2014) attributed the formation of SASTMW3 to the Brazil Current and its interaction with the Subtropical Front. In addition, the general surface and subsurface geographical distribution of the three mode water varieties in Sato and Polito (2014) differs from the present study. Here, the surface expression of SASTMW1 occupies the entire region of the southern limit of the subtropical gyre, between the Brazil-Malvinas Confluence and the 0° meridian, while the subsurface SASMTW1 extends across the entire subtropical gyre. In Sato and Polito (2014), the zonal spreading of SAST-MW1 is less expanded. The opposite is also observed for the densest subsurface SASTMW variety, SASTMW3, that in our study it is delimited to the eastern half of the basin and extends slightly westward of the Mid-Atlantic Ridge, whereas in Sato and Polito (2014), the subsurface SASTMW3 was found up to 40°W as its western limit.

These discrepancies might be due to the different methods of determination used to define both, the surface mixed layers and mode waters. The SASTMW selection criteria of Sato and Polito (2014) are limitations on potential vorticity ($|q| <= 1.50 \times 10^{-10}$ m^{-1} s^{-1}), potential temperature (11.5−18.5°C) and salinity (34.7−36.5 psu). The last two limitations also led to a density range of 25.6–26.8 kg m^{-3} as well as a temperature gradient less than 0.01°C m^{-1}. After applying those strict criteria, their analysis resulted in two configurations of the vertical

(surface and subsurface mode waters). The surface mode water that represents the formation process was compared to the local climatological maximum MLD (Holte & Talley, 2009) to distinguish it from a regular mixed layer. In the current study, both the surface MLD and lower boundary of mode water are detected at the depth of extreme curvatures. While MLDs are estimated from density profiles, mode water layers, on the other hand, are derived from temperature profiles in addition to a universal limitation on potential vorticity. Outcropping mode waters are simply defined as temperature-based mixed layers thicker than 100 dbar, yet still show the most frequent occurrence between winter and early spring.

Another focus in this study is on the relationship between mesoscale eddies and mode waters. Here, we apply the recently developed eddy-detection TOEddies algorithm (Laxenaire et al., 2018) that objectively defines eddies from satellite altimetry maps of ADT. The resulting eddies are then co-located with Argo profiles. Although TOEddies provides 2D daily eddy fields that enable to access the horizontal distribution of eddies and their complex trajectories, its ability to include the whole spectrum of eddies is limited. This limitation is not only due to the spatio-temporal resolution of the altimetry fields, but also to the fact that only when subsurface features have a signature in altimetry maps can they be detected. In this study, we applied a second method to determine the presence of eddies and their depth extent directly from Argo data by constructing vertical profiles of SHA. We used it to separate subsurface eddies from surface ones when the profile has already been co-located with an altimeter-detected eddy. Such SHA separation provides only sparse observations of the eddy fields, which does not allow to reconstruct the 3D eddy structure alone, but it enables to better assess the presence of subsurface features. In the study, TOEddies allows us to obtain the South Atlantic eddy characteristics and main propagation pathways, while the SHA method provides supplementary information of subsurface-intensified eddies.

The Argo-TOEddies co-location provides a lower percentage of eddies sampled by Argo profilers than that of Sato and Polito (2014). Though both studies show that Argo profilers are indifferent to the presence of mesoscale eddies, eddy-mode water co-location in the current study exhibits higher percentage (41.6% of mode waters falling in eddies in this study against 22.4% for Sato & Polito, 2014 who used the Chelton et al., 2011 eddy climatology). The study also suggests a particularly large amount of mode water presence associated with TOEddies anticyclonic eddies and their transport as coherent structures (32.0% inside anticyclones and 9.6% inside cyclones). The study of Sato and Polito (2014) divided the total number into surface and subsurface mode waters, and in both cases, the co-located anticyclones outnumbered cyclones by nearly 4 to 1. Moreover, the SHA eddy separation method brings an additional perspective. Not all TOEddies-detected eddies are separable into surface-intensified and subsurface-intensified eddies (93.3% of all eddies were separated), but more subsurface mode waters are captured by subsurface eddies. Hence, our results indicate a clear influence of mesoscale dynamics and, in particular, of anticyclonic eddies on the formation, transport, and subduction of mode waters in the subtropical gyre interior of the South Atlantic.

Moreover, the analysis of temperature anomalies along isopycnals related to the detected subtropical mode waters shows that mode waters carry heat from the surface subtropical gyre edges into the gyre's interior. Laxenaire et al. (2020) suggested that Agulhas Rings transport heat efficiently into the South Atlantic subtropical gyre, with heat anomalies centered in the mode water layers. The present study generalizes these results to the entire scope of the SASTMW, with anticyclonic eddies playing an important role in ventilating the upper South Atlantic thermocline and advecting heat in the subtropical gyre interior.

In general, the present study offers an improved understanding of subtropical mode waters in the South Atlantic. Despite the qualitative agreement between the pattern of eddy presence and spatial distribution of mode waters, the new algorithm has a number of facts to improve. The identification of pycnocline and thermocline is interpreted as the lower boundary of mixed layer detection, and thus is a rather poor representation. In addition, there has been a dilemma when it comes to choose whether the calculation should be based on temperature or density profiles. The surface mixed layer is commonly defined by strong convection that is better detected from density, while mode water is frequently observed as a specific water mass and sometimes a remarkably uniform density profile results from a compensation between salinity and temperature. This study thus depends on both temperature and density homogeneity to identify mode waters, and refers to density to define the MLD. A similar selecting process following Holte and Talley (2009) to find the best estimate of MLDs could also be added to the current algorithm for (a) comparing with other mixed layer definitions, and (b) providing an ensemble of several mode water identification methods (e.g., the temperature method based on CLT with layer thickness control, or a single application of potential vorticity threshold to define mode waters).

Studies on global mode water analysis (Feucher et al., 2019; Tsubouchi et al., 2016) usually compare spatial structures of mode waters in different basins; however, the effect of mesoscale eddies is not extensively taken into consideration, while other studies that concentrate on the dynamical explanation concerning the relationship between mode waters and eddies generally delimit to specific conditions and locations (Qiu et al., 2007). Our algorithm for mode water detection and the co-location with eddies will allow an extension to other observational platforms and to other domains of interest. This algorithm was also validated by applying it to several hydrographic CTD profiles in the South Atlantic region (not shown). Combined with bottle data of carbon and oxygen, we will be able to obtain the link between mode waters and several other biogeochemical properties.

With the combination of thickness and area, it is also of interest to calculate the volume distribution associated with each type of mode water. Such calculation was considered by Bernardo and Sato (2020) that draws a volumetric picture of the three SASTMW types clustered in Sato and Polito (2014). Subsequently, another important characteristic associated with mode water, the volume transport starting from their original regions of formation to the areas of spreading, can be calculated and evaluated at the global scale. Regarding the important role that eddies play in mode water transport, the calculation of mode water volume transport can thus be achieved by accurately tracking coherent eddies and computing the momentum changes along the eddy tracks. This will allow us to understand to what extent eddies transport mode waters and how much of mode waters dissipate associated with these eddy trajectories. However, such estimates can be roughly approximated only by using altimetry eddy detection together with vertical profiles provided by Argo or other platforms. Indeed, for eddies detected by satellite altimetry, we can gather information on the eddy size and shape whereas this information is not available from eddies that are detected by sparse vertical profiles (e.g., the SHA method we implemented here [if applied alone to detect eddies]).

In this study, the SHA method was applied to distinguish subsurface eddies from surface ones. However, the applicability of this method greatly depends on vertical scales of these eddies, and sampling rates of temperature and salinity data. This profile-only method could also be applied to detect eddies alone, yet it highly requires verification and comparison with other more traditional satellite-based eddy detection methods. Considering the large number of eddies that can be detected from the SHA method, the dependence of eddy determination on several aspects of the SHA needs to be tested further, for example, the choice of climatological profile to deduct, the minimum magnitude of SHA to be identified as an eddy, and the threshold depth that separates subsurface eddies from surface ones. It will also be of interest to look into numerical results to visualize and analyze the relationship between mode waters and several small-scale mechanisms.

Appendix A: Eddy Detection From the Steric Height Anomaly

In this study, we mainly applied the TOEddies detection algorithm to detect eddies from the sea surface ADT, and then co-located them with Argo profiles. Subsequently, the SHA for each Argo profile is calculated to determine whether the specific co-located eddy is surface- or subsurface-intensified; nonetheless, the vertical location of some profiles is unidentified from the SHA method. At the same time, we also acknowledge that satellite altimetry does not always provide precise detection since eddies can evolve as subsurface eddies when they relocate. Only when these subsurface ones still have a surface signature can they be detected from satellites. Accordingly, in this Appendix, we show the possibility of using SHA alone to detect eddies, without any altimetry-based detection in advance.

In general, this SHA method implies that each Argo profile makes up one eddy detection, which seems unrealistic. However, it might be appealing to apply this SHA detection method to Argo profiles that are already detected with mode waters, since the homogeneity of mode waters implies less mixing in progress at the core both horizontally and vertically, which refers to specific features like mesoscale eddies. Figure A1 shows patterns of eddy-mode water co-location as a comparison between TOEddies and SHA eddy detection methods. Left and middle panels display respectively TOEddies- and SHA-detected surface eddies (co-located with both outcropping and subsurface mode waters), which suggest that these two methods are comparable. It also provides some confidence for using SHA to analyze the co-location between eddies and mode waters. At the same time, TOEddies detection generally leads to a larger number of eddy-mode water co-location than that of the SHA surface eddy detection, except that outcropping mode waters inside SHA-detected surface anticyclones (Figure A1e) outnumber those inside TOEddies-derived anticyclones (Figure A1d) by more than 1000. The outnumbered

co-location between TOEddies and mode waters confirms that detection methods based on altimeters are to some extent capable of identifying subsurface-intensified eddies. From another point of view, the difference between the TOEddies and SHA detection methods is dependent on the depth threshold of the maximum SHA that is used in the latter to distinguish subsurface eddies from surface ones. In other words, this depth threshold determines the proportion of surface- and subsurface-intensified eddies, as the comparison between the numbers of profiles shown in the middle and right panels of Figure A1. Moreover, the percentage of profiles containing SASTMW yet indiscernible from the SHA surface eddy detection is very small (31.8% inside cyclones, 63.2% inside anti-cyclones, and only 5.0% that is unknown from the calculation), in contrast with the resulting percentage of mode waters outside of TOEddies detection (58.4%).

Another climatological profiling data set was also applied to replace the one from the TOEddies atlas that was subtracted from the original σ_0 profile to calculate SHA, that is, the monthly mean profile (averaged over 2005–2017 years) retrieved from the 1/4° gridded World Ocean Atlas 2018 (WOA18). For the application of this climatology, the calculation of σ_0' is thus accomplished by looking for the closest WOA18 profile to each Argo profile in the geographical coordinate. However, we find the calculation of SHA highly depends on the choices
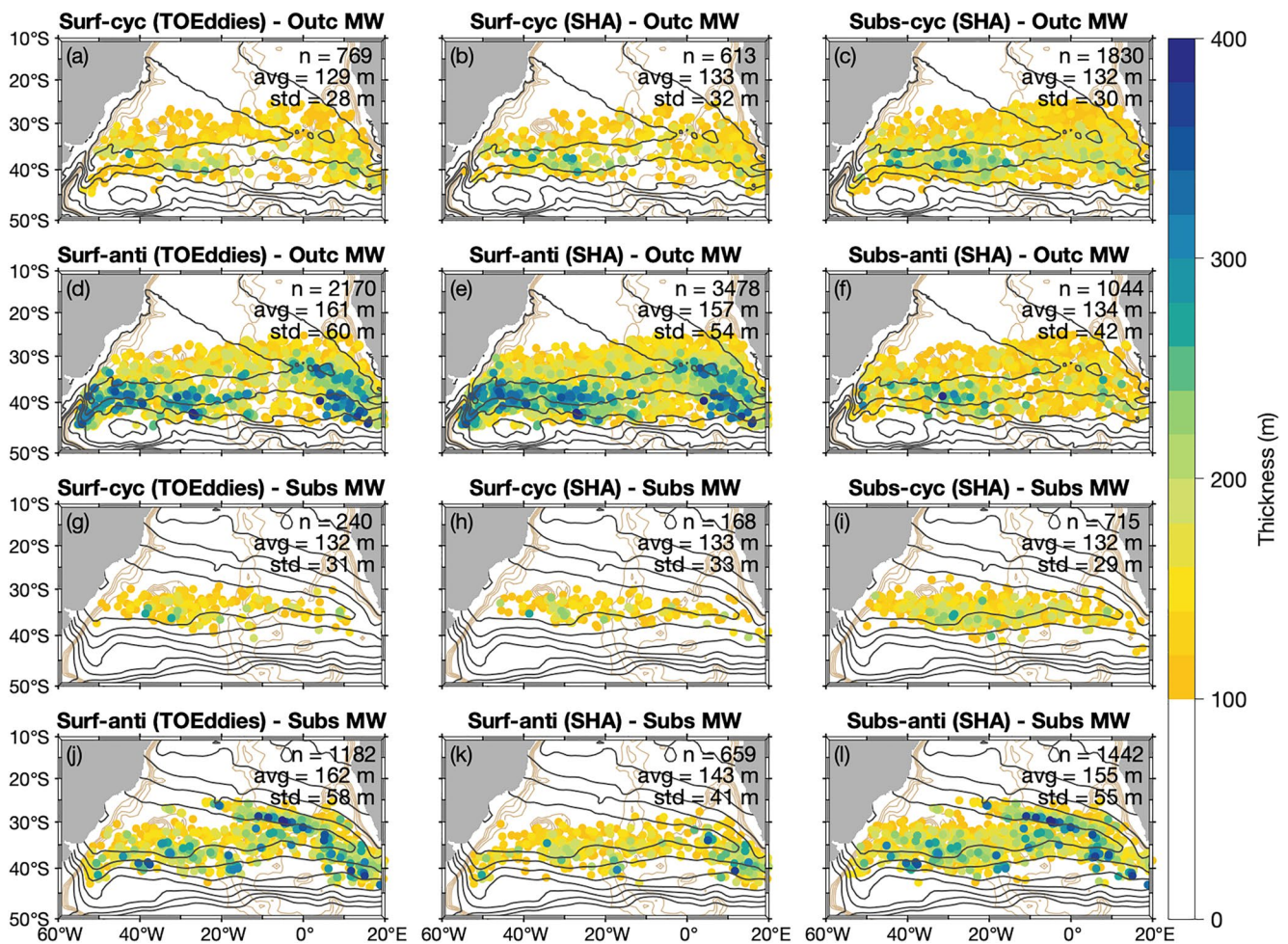

Figure A1. The co-location between mesoscale eddies and mode waters. Left panels (a/d/g/j) show mode waters associated with the TOEddies detection applied to absolute dynamic topography (ADT) maps; middle (b/e/h/k) and right (c/f/i/l) panels show mode waters inside eddies that are detected by the steric height anomaly (SHA). Since the calculation of SHA is mainly used to distinguish subsurface-intensified eddies from surface ones, panels (b/e/h/k) display mode waters associated with surface-intensified eddies whereas panels (c/f/i/l) show mode waters related to subsurface-intensified eddies. The numbers marked by *n*, *avg*, and *std* are respectively indicative of the total number, mean value, and standard deviation of mode water thicknesses. The gray contours in the panels of the upper two rows indicate the mean dynamic topography (MDT) as an estimate of the mean sea surface height above geoid over the 1993–2012 period (Mulet et al., 2021), whereas in the panels of the lower two rows they represent the steric height (anomaly) contours at 400 dbar integrated from 1,200 dbar and averaged in each 1° × 1° grid. The light brown contours show bathymetry over −3,600 to −1,800 m.

of climatology. Recalling Figure 3 that shows three example profiles of mode water detection, we find the (c/d) profile is co-located with a TOEddies-detected anticyclonic Agulhas Ring. By calculating SHAs, the other two profiles (a/b) and (e/f) are also co-located with anticyclonic eddies, albeit they have not been identified as such from the TOEddies method. However, when the WOA18 climatology is employed instead of the TOEddies climatology, these two profiles are instead detected as surface cyclones. Though it seems plausible to assume that both (a/b) and (e/f) are co-located with anticyclonic eddies since both profiles hold thick mode water layers, the dependence of eddy detection on climatologies makes the result more ambiguous. We found this ambiguity results from the assumption that the pressure of 1,500 dbar is regarded as the no-motion reference level. However, it is not the case when WOA18 climatology is applied to calculate the SHA in that at the lowest depth, a relatively large difference is observed for the comparison between the WOA18 value and the Argo profile value. This indicates that the WOA18 climatology is not the optimal choice, even though we apply the monthly mean climatology with 1/4° as resolution.

Briefly, the eddy detection with this steric height method gives an alternative definition of eddies with respect to the satellite altimetry, and its combination with mode water detection provides an opportunity to use only Argo profiles to quantify the influence of eddies on mode water formation and variability. Whichever eddy detection method is combined with mode waters, anticyclonic eddies predominantly contain more than two folds of mode waters than cyclonic eddies. However, the SHA lacks verification to be used alone to detect eddies and it is also noteworthy that steric height anomalies might also represent signatures of internal waves (Dilmahamod et al., 2018). Further tests on the choices of climatological profile, the minimum magnitude of SHA to be identified as an eddy, and the threshold depth that separates subsurface eddies from surface ones are required.

Appendix B: An Average Picture of Different MLD Detection Methods

We recognize that our curvature-based method in Figure 4d results in a very similar MLD detection to the threshold method of (a), with around 79.1% of all profiles identified with the same depths. It is thus plausible to indicate a similar dependence of the new algorithm on density threshold $\sigma_{0th} = 0.03$ kg m^{-3}, though the latter threshold was applied as a gatekeeper to validate the mixed layer estimates that are homogeneous enough. Table 2 provides similar information, as well as another detail that our algorithm leads to a higher standard deviation of the three boxes. We admit that the comparison of different MLD detection methods lacks some statistical proofs to point out which approach brings the best estimate, that is, more precise. However, the curvature-dependent detection gives an individual calculation for each profile, which in theory, results in more diverse MLDs, that is, higher standard deviation associated with a spatial average. Figure B1 shows the domain-averaged profiles of potential temperature (black), salinity (red), and potential density (blue) of the three boxes in Figure 4a, so as to compare five MLD detecting methods. From the perspective of spatial averages, it is true that the detection based on gradient limits results in a thinner mixed layer compared with density or temperature threshold method. Focused on the calculation from density profiles, our curvature detection leads to a deeper MLD than the density gradient method and a shallower depth compared to the density threshold approach. In spite of such interpretation, it is still necessary to systematically prove which MLD detection is more precise.
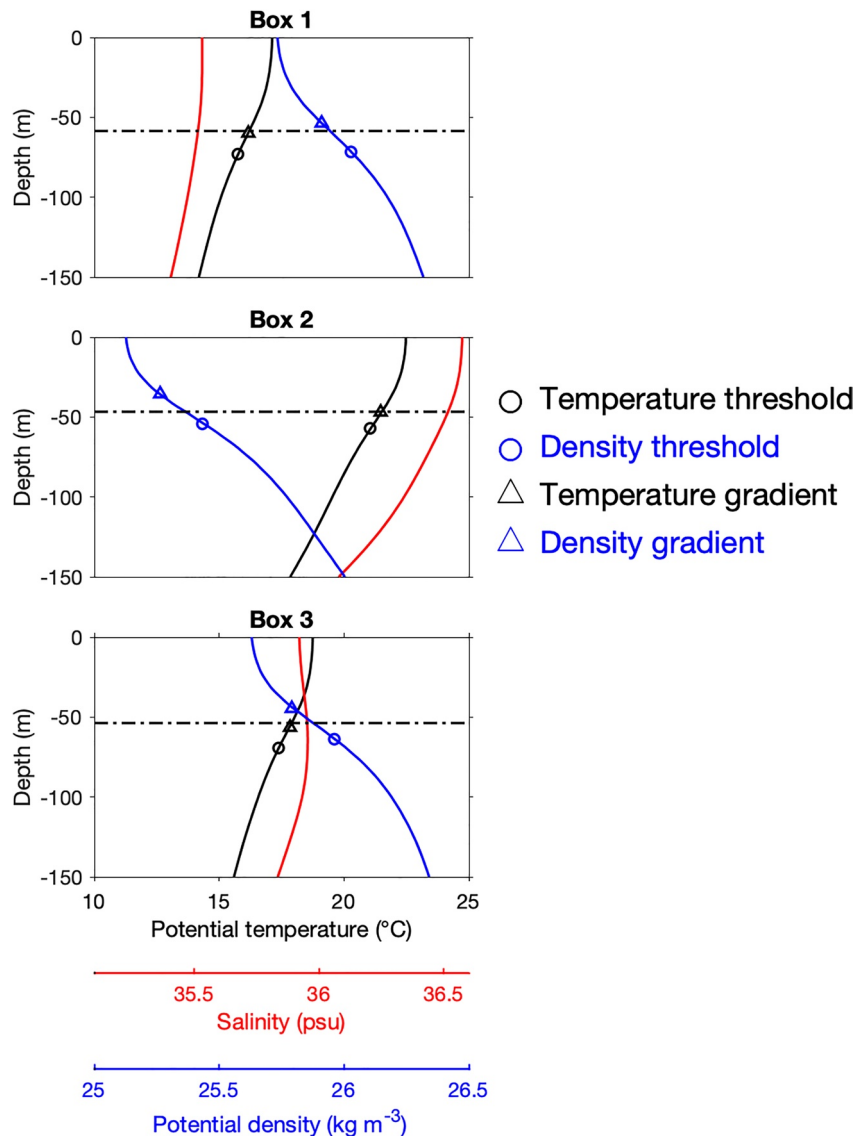
Figure B1. The averaged profiles circumscribed by three boxes in Figure 4a, with depth locations of different mixed layer depths (MLDs). The black dash-dot lines indicate the new algorithm's results that are dependent on curvature. The other methods of MLD detection are marked by circles (for threshold methods) or triangles (for density threshold methods) in the figure.

Data Availability Statement

The availability of the following products used in this study is also appreciated: the Argo data from the Coriolis Center (http://www.coriolis.eu.org); altimeter merged products by AVISO (http://www.aviso.oceanobs.com); the global ocean heat fluxes provided by the WHOI OAFlux project (http://oaflux.whoi.edu); and the eddy detection algorithm and atlas TOEddies developed by Laxenaire et al. (2018).

References

Akima, H. (1970). A new method of interpolation and smooth curve fitting based on local procedures. *Journal of the Association for Computing Machinery*, *17*(4), 589–602. https://doi.org/10.1145/321607.321609

Alexander, M. A., & Deser, C. (1995). A mechanism for the recurrence of wintertime midlatitude sst anomalies. *Journal of Physical Oceanography*, *25*(1), 122–137. https://doi.org/10.1175/1520-0485(1995)025<0122:AMFTRO>2.0.CO;2

Argo. (2020). Argo float data and metadata from global data assembly centre (argo gdac) [Dataset]. Retrieved from http://www.coriolis.eu.org. https://doi.org/10.17882/42182

Assassi, C., Morel, Y., Vandermeirsch, F., Chaigneau, A., Pegliasco, C., Morrow, R., & Cambra, R. (2016). An index to distinguish surface- and subsurface-intensified vortices from surface observations. *Journal of Physical Oceanography*, *46*(8), 2529–2552. https://doi.org/10.1175/JPO-D-15-0122.1

Bachman, S. D., Taylor, J. R., Adams, K. A., & Hosegood, P. J. (2017). Mesoscale and submesoscale effects on mixed layer depth in the southern ocean. *Journal of Physical Oceanography*, *47*(9), 2173–2188. https://doi.org/10.1175/JPO-D-17-0034.1

Bashmachnikov, I., & Carton, X. (2012). Surface signature of Mediterranean water eddies in the northeastern Atlantic: Effect of the upper ocean stratification. *Ocean Science*, *8*(6), 931–943. https://doi.org/10.5194/os-8-931-2012

Bates, N. R., Pequignet, A. C., Johnson, R. J., & Gruber, N. (2002). A short-term sink for atmospheric CO2 in subtropical mode water of the North Atlantic Ocean. *Nature*, *420*(6915), 489–493. https://doi.org/10.1038/nature01253

Bernardo, P. S., & Sato, O. T. (2020). Volumetric characterization of the South Atlantic subtropical mode water types. *Geophysical Research Letters*, *47*(8), e2019GL086653. https://doi.org/10.1029/2019GL086653

Boyer, T. P., Garcia, H. E., Locarnini, R. A., Zweng, M. M., Mishonov, A. V., Reagan, J. R., & Smolyar, I. V. (2019). *World ocean atlas 2018*. NOAA National Centers for Environmental Information. Retrieved from https://accession.nodc.noaa.gov/NCEI-WOA18

Capuano, T. A., Speich, S., Carton, X., & Laxenaire, R. (2018). Indo-atlantic exchange, mesoscale dynamics, and antarctic intermediate water. *Journal of Geophysical Research: Oceans*, *123*(5), 3286–3306. https://doi.org/10.1002/2017JC013521

Chaigneau, A., Le Texier, M., Eldin, G., Grados, C., & Pizarro, O. (2011). Vertical structure of mesoscale eddies in the eastern South Pacific Ocean: A composite analysis from altimetry and argo profiling floats. *Journal of Geophysical Research: Oceans*, *116*(C11). https://doi.org/10.1029/2011JC007134

Chelton, D. B., Schlax, M. G., & Samelson, R. M. (2011). Global observations of nonlinear mesoscale eddies. *Progress in Oceanography*, *91*(2), 167–216. https://doi.org/10.1016/j.pocean.2011.01.002

Cheng, L., Trenberth, K. E., Fasullo, J., Boyer, T., Abraham, J., & Zhu, J. (2017). Improved estimates of ocean heat content from 1960 to 2015. *Science Advances*, *3*(3). https://doi.org/10.1126/sciadv.1601545

Davis, X. J., Rothstein, L. M., Dewar, W. K., & Menemenlis, D. (2011). Numerical investigations of seasonal and interannual variability of north pacific subtropical mode water and its implications for pacific climate variability. *Journal of Climate*, *24*(11), 2648–2665. https://doi.org/10.1175/2010JCLI3435.1

de Boyer Montégut, C., Madec, G., Fischer, A. S., Lazar, A., & Iudicone, D. (2004). Mixed layer depth over the global ocean: An examination of profile data and a profile-based climatology. *Journal of Geophysical Research: Oceans*, *109*(C12). https://doi.org/10.1029/2004JC002378

de Souza, A. G. Q., Kerr, R., & de Azevedo, J. L. L. (2018). On the influence of subtropical mode water on the South Atlantic Ocean. *Journal of Marine Systems*, *185*, 13–24. https://doi.org/10.1016/j.jmarsys.2018.04.006

Dencausse, G., Arhan, M., & Speich, S. (2010). Routes of agulhas rings in the southeastern Cape Basin. *Deep Sea Research Part I: Oceanographic Research Papers*, *57*(11), 1406–1421. https://doi.org/10.1016/j.dsr.2010.07.008

Deser, C., Alexander, M. A., & Timlin, M. S. (2003). Understanding the persistence of sea surface temperature anomalies in midlatitudes. *Journal of Climate*, *16*(1), 57–72. https://doi.org/10.1175/1520-0442(2003)016<0057:UTPOSS>2.0.CO;2

DeVries, T. (2014). The oceanic anthropogenic CO2 sink: Storage, air-sea fluxes, and transports over the industrial era. *Global Biogeochemical Cycles*, *28*(7), 631–647. https://doi.org/10.1002/2013GB004739

Dilmahamod, A. F., Aguiar-González, B., Penven, P., Reason, C. J. C., De Ruijter, W. P. M., Malan, N., & Hermes, J. C. (2018). Siddies corridor: A major east-west pathway of long-lived surface and subsurface eddies crossing the subtropical South Indian Ocean. *Journal of Geophysical Research: Oceans*, *123*(8), 5406–5425. https://doi.org/10.1029/2018JC013828

Dong, S., Sprintall, J., Gille, S. T., & Talley, L. (2008). Southern ocean mixed-layer depth from argo float profiles. *Journal of Geophysical Research: Oceans*, *113*(C6). https://doi.org/10.1029/2006JC004051

Droghei, R., Buongiorno Nardelli, B., & Santoleri, R. (2018). A new global sea surface salinity and density dataset from multivariate observations (1993–2016). *Frontiers in Marine Science*, *5*, 84. https://doi.org/10.3389/fmars.2018.00084

Dufois, F., Hardman-Mountford, N. J., Greenwood, J., Richardson, A. J., Feng, M., & Matear, R. J. (2016). Anticyclonic eddies are more productive than cyclonic eddies in subtropical gyres because of winter mixing. *Science Advances*, *2*(5). https://doi.org/10.1126/sciadv.1600282

Feucher, C., Maze, G., & Mercier, H. (2016). Mean structure of the north atlantic subtropical permanent pycnocline from in situ observations. *Journal of Atmospheric and Oceanic Technology*, *33*(6), 1285–1308. https://doi.org/10.1175/JTECH-D-15-0192.1

Feucher, C., Maze, G., & Mercier, H. (2019). Subtropical mode water and permanent pycnocline properties in the world ocean. *Journal of Geophysical Research: Oceans*, *124*(2), 1139–1154. https://doi.org/10.1029/2018JC014526

Friedlingstein, P., O'Sullivan, M., Jones, M. W., Andrew, R. M., Hauck, J., Olsen, A., & Zaehle, S. (2020). Global carbon budget 2020. *Earth System Science Data*, *12*(4), 3269–3340. https://doi.org/10.5194/essd-12-3269-2020

Gaube, P., McGillicuddy, D. J., Jr, & Moulin, A. J. (2019). Mesoscale eddies modulate mixed layer depth globally. *Geophysical Research Letters*, *46*(3), 1505–1512. https://doi.org/10.1029/2018GL080006

Gill, A., & Niller, P. (1973). The theory of the seasonal variability in the ocean. *Deep Sea Research and Oceanographic Abstracts*, *20*(2), 141–177. https://doi.org/10.1016/0011-7471(73)90049-1

Gordon, A. L. (1989). Brazil-Malvinas confluence–1984. *Deep Sea Research Part A: Oceanographic Research Papers*, *36*(3), 359–384. https://doi.org/10.1016/0198-0149(89)90042-3

Gordon, A. L., Weiss, R. F., Smethie, W. M., Jr, & Warner, M. J. (1992). Thermocline and intermediate water communication between the South Atlantic and Indian oceans. *Journal of Geophysical Research*, *97*(C5), 7223–7240. https://doi.org/10.1029/92JC00485

Guerra, L. A. A., Paiva, A. M., & Chassignet, E. P. (2018). On the translation of Agulhas rings to the western South Atlantic Ocean. *Deep Sea Research Part I: Oceanographic Research Papers*, *139*, 104–113. https://doi.org/10.1016/j.dsr.2018.08.005

Hanawa, K., & Sugimoto, S. (2004). 'reemergence' areas of winter sea surface temperature anomalies in the world's oceans. *Geophysical Research Letters*, *31*(10). https://doi.org/10.1029/2004GL019904

Hanawa, K., & Talley, L. D. (2001). Chapter 5.4 – Mode waters. In *Ocean circulation and climate* (Vol. 77, p. 373–386). Academic Press. https://doi.org/10.1016/S0074-6142(01)80129-7

Hautala, S. L., & Roemmich, D. H. (1998). Subtropical mode water in the northeast Pacific basin. *Journal of Geophysical Research: Oceans*, *103*(C6), 13055–13066. https://doi.org/10.1029/98JC01015

Herraiz-Borreguero, L., & Rintoul, S. R. (2011). Subantarctic mode water: Distribution and circulation. *Ocean Dynamics*, *61*(1), 103–126. https://doi.org/10.1007/s10236-010-0352-9

Holte, J., & Talley, L. (2009). A new algorithm for finding mixed layer depths with applications to argo data and subantarctic mode water formation. *Journal of Atmospheric and Oceanic Technology*, *26*(9), 1920–1939. https://doi.org/10.1175/2009JTECHO543.1

Kara, A. B., Rochford, P. A., & Hurlburt, H. E. (2000). Mixed layer depth variability and barrier layer formation over the North Pacific Ocean. *Journal of Geophysical Research*, *105*(C7), 16783–16801. https://doi.org/10.1029/2000JC900071

Kouketsu, S., Tomita, H., Oka, E., Hosoda, S., Kobayashi, T., & Sato, K. (2012). The role of meso-scale eddies in mixed layer deepening and mode water formation in the western North Pacific. *Journal of Oceanography*, *68*(1), 63–77. https://doi.org/10.1007/s10872-011-0049-9

Kwon, Y.-O., & Riser, S. C. (2004). North Atlantic subtropical mode water: A history of Ocean-atmosphere interaction 1961–2000. *Geophysical Research Letters*, *31*(19). https://doi.org/10.1029/2004GL021116

Laxenaire, R., Speich, S., Blanke, B., Chaigneau, A., Pegliasco, C., & Stegner, A. (2018). Anticyclonic eddies connecting the western boundaries of Indian and Atlantic oceans. *Journal of Geophysical Research: Oceans*, *123*(11), 7651–7677. https://doi.org/10.1029/2018JC014270

Laxenaire, R., Speich, S., & Stegner, A. (2019). Evolution of the thermohaline structure of one Agulhas ring reconstructed from satellite altimetry and argo floats. *Journal of Geophysical Research: Oceans*, *124*(12), 8969–9003. https://doi.org/10.1029/2018JC014426

Laxenaire, R., Speich, S., & Stegner, A. (2020). Agulhas ring heat content and transport in the South Atlantic estimated by combining satellite altimetry and argo profiling floats data. *Journal of Geophysical Research: Oceans*, *125*(9), e2019JC015511. https://doi.org/10.1029/2019JC015511

Levitus, S., Antonov, J. I., Boyer, T. P., Baranova, O. K., Garcia, H. E., Locarnini, R. A., & Zweng, M. M. (2012). World ocean heat content and thermosteric sea level change (0–2000 m), 1955–2010. *Geophysical Research Letters*, *39*(10). https://doi.org/10.1029/2012GL051106

Lloyd, S. (1982). Least squares quantization in PCM. *IEEE Transactions on Information Theory*, *28*(2), 129–137. https://doi.org/10.1109/TIT.1982.1056489

Lorbacher, K., Dommenget, D., Niiler, P. P., & Köhl, A. (2006). Ocean mixed layer depth: A subsurface proxy of Ocean-atmosphere variability. *Journal of Geophysical Research*, *111*(C7). https://doi.org/10.1029/2003JC002157

Marshall, D. (1997). Subduction of water masses in an eddying ocean. *Journal of Marine Research*, *55*(2), 201–222. https://doi.org/10.1357/0022240973224373

McCoy, D., Bianchi, D., & Stewart, A. L. (2020). Global observations of submesoscale coherent vortices in the ocean. *Progress in Oceanography*, *189*, 102452. https://doi.org/10.1016/j.pocean.2020.102452

Merchant, C. J., Embury, O., Bulgin, C. E., Block, T., Corlett, G. K., Fiedler, E., & Donlon, C. (2019). Satellite-based time-series of sea-surface temperature since 1981 for climate applications. *Scientific Data*, *6*(1), 223. https://doi.org/10.1038/s41597-019-0236-x

Mulet, S., Rio, M.-H., Etienne, H., Artana, C., Cancet, M., Dibarboure, G., & Strub, P. T. (2021). The new CNES-CLS18 global mean dynamic topography. *Ocean Science Discussions*, *2021*, 1–31. https://doi.org/10.5194/os-2020-117

Nakamura, H. (1996). A pycnostad on the bottom of the ventilated portion in the central subtropical North Pacific: Its distribution and formation. *Journal of Oceanography*, *52*(2), 171–188. https://doi.org/10.1007/BF02235668

Nishikawa, S., Tsujino, H., Sakamoto, K., & Nakano, H. (2010). Effects of mesoscale eddies on subduction and distribution of subtropical mode water in an eddy-resolving OGCM of the western North Pacific. *Journal of Physical Oceanography*, *40*(8), 1748–1765. https://doi.org/10.1175/2010JPO4261.1

Oka, E., Kouketsu, S., Toyama, K., Uehara, K., Kobayashi, T., Hosoda, S., & Suga, T. (2011). Formation and subduction of central mode water based on profiling float data, 2003–08. *Journal of Physical Oceanography*, *41*(1), 113–129. https://doi.org/10.1175/2010JPO4419.1

Park, S., Deser, C., & Alexander, M. A. (2005). Estimation of the surface heat flux response to sea surface temperature anomalies over the global oceans. *Journal of Climate*, *18*(21), 4582–4599. https://doi.org/10.1175/JCLI3521.1

Pegliasco, C., Chaigneau, A., & Morrow, R. (2015). Main eddy vertical structures observed in the four major eastern boundary upwelling systems. *Journal of Geophysical Research: Oceans*, *120*(9), 6008–6033. https://doi.org/10.1002/2015JC010950

Provost, C., Escoffier, C., Maamaatuaiahutapu, K., Kartavtseff, A., & Garçon, V. (1999). Subtropical mode waters in the South Atlantic Ocean. *Journal of Geophysical Research*, *104*(C9), 21033–21049. https://doi.org/10.1029/1999JC900049

Pujol, M.-I., Faugère, Y., Taburet, G., Dupuy, S., Pelloquin, C., Ablain, M., & Picot, N. (2016). DUACS DT2014: The new multi-mission altimeter data set reprocessed over 20 years. *Ocean Science*, *12*(5), 1067–1090. https://doi.org/10.5194/os-12-1067-2016

Qiu, B., & Chen, S. (2006). Decadal variability in the formation of the North Pacific subtropical mode water: Oceanic versus atmospheric control. *Journal of Physical Oceanography*, *36*(7), 1365–1380. https://doi.org/10.1175/JPO2918.1

Qiu, B., Chen, S., & Hacker, P. (2007). Effect of mesoscale eddies on subtropical mode water variability from the Kuroshio extension system study (KESS). *Journal of Physical Oceanography*, *37*(4), 982–1000. https://doi.org/10.1175/JPO3097.1

Qu, T., Xie, S.-P., Mitsudera, H., & Ishida, A. (2002). Subduction of the North Pacific mode waters in a global high-resolution GCM. *Journal of Physical Oceanography*, *32*(3), 746–763. https://doi.org/10.1175/1520-0485(2002)032<0746:SOTNPM>2.0.CO;2

Roemmich, D., & Cornuelle, B. (1992). The subtropical mode waters of the South Pacific Ocean. *Journal of Physical Oceanography*, *22*(10), 1178–1187. https://doi.org/10.1175/1520-0485(1992)022<1178:TSMWOT>2.0.CO;2

Sabine, C. L., Feely, R. A., Gruber, N., Key, R. M., Lee, K., Bullister, J. L., & Rios, A. F. (2004). The oceanic sink for anthropogenic CO2. *Science*, *305*(5682), 367–371. https://doi.org/10.1126/science.1097403

Sato, K., Suga, T., & Hanawa, K. (2006). Barrier layers in the subtropical gyres of the world's oceans. *Geophysical Research Letters*, *33*(8). https://doi.org/10.1029/2005GL025631

Sato, O. T., & Polito, P. S. (2014). Observation of South Atlantic subtropical mode waters with argo profiling float data. *Journal of Geophysical Research: Oceans*, *119*(5), 2860–2881. https://doi.org/10.1002/2013JC009438

Schmidtko, S., Johnson, G. C., & Lyman, J. M. (2013). MIMOC: A global monthly isopycnal upper-ocean climatology with mixed layers. *Journal of Geophysical Research: Oceans*, *118*(4), 1658–1672. https://doi.org/10.1002/jgrc.20122

Schütte, F., Brandt, P., & Karstensen, J. (2016). Occurrence and characteristics of mesoscale eddies in the tropical northeastern atlantic ocean. *Ocean Science*, *12*(3), 663–685. https://doi.org/10.5194/os-12-663-2016

Smith, W. H. F., & Sandwell, D. T. (1997). Global sea floor topography from satellite altimetry and ship depth soundings. *Science*, *277*(5334), 1956–1962. https://doi.org/10.1126/science.277.5334.1956

Spall, M. A. (1995). Frontogenesis, subduction, and cross-front exchange at upper ocean fronts. *Journal of Geophysical Research: Oceans*, *100*(C2), 2543–2557. https://doi.org/10.1029/94JC02860

Speer, K., & Forget, G. (2013). Chapter 9—Global distribution and formation of mode waters. In *Ocean circulation and climate* (Vol. 103, pp. 211–226). Academic Press. https://doi.org/10.1016/B978-0-12-391851-2.00009-X

Speich, S., Blanke, B., & Cai, W. (2007). Atlantic meridional overturning circulation and the southern hemisphere supergyre. *Geophysical Research Letters*, *34*(23). https://doi.org/10.1029/2007GL031583

Sprintall, J., & Tomczak, M. (1992). Evidence of the barrier layer in the surface layer of the tropics. *Journal of Geophysical Research*, *97*(C5), 7305–7316. https://doi.org/10.1029/92JC00407

Stramma, L., & England, M. (1999). On the water masses and mean circulation of the South Atlantic ocean. *Journal of Geophysical Research*, *104*(C9), 20863–20883. https://doi.org/10.1029/1999JC900139

Suga, T., & Hanawa, K. (1990). The mixed-layer climatology in the northwestern part of the North Pacific subtropical gyre and the formation area of subtropical mode water. *Journal of Marine Research*, *48*(3), 543–566. https://doi.org/10.1357/002224090784984669

Talley, L. D., Pickard, G. L., Emery, W. J., & Swift, J. H. (2011). Chapter 9—Atlantic ocean. In L. D. Talley, G. L. Pickard, W. J. Emery, & J. H. Swift (Eds.), *Descriptive physical oceanography* (6th ed., pp. 245–301). Academic Press. https://doi.org/10.1016/B978-0-7506-4552-2.10009-5

Tsubouchi, T., Suga, T., & Hanawa, K. (2007). Three types of South Pacific subtropical mode waters: Their relation to the large-scale circulation of the South Pacific subtropical gyre and their temporal variability. *Journal of Physical Oceanography*, *37*(10), 2478–2490. https://doi.org/10.1175/JPO3132.1

Tsubouchi, T., Suga, T., & Hanawa, K. (2010). Indian Ocean subtropical mode water: Its water characteristics and spatial distribution. *Ocean Science*, *6*(1), 41–50. https://doi.org/10.5194/os-6-41-2010

Tsubouchi, T., Suga, T., & Hanawa, K. (2016). Comparison study of subtropical mode waters in the world ocean. *Frontiers in Marine Science*, *3*, 270. https://doi.org/10.3389/fmars.2016.00270

Uehara, H., Suga, T., Hanawa, K., & Shikama, N. (2003). A role of eddies in formation and transport of North Pacific subtropical mode water. *Geophysical Research Letters*, *30*(13). https://doi.org/10.1029/2003GL017542

von Schuckmann, K., Cheng, L., Palmer, M. D., Hansen, J., Tassone, C., Aich, V., & Wijffels, S. E. (2020). Heat stored in the earth system: Where does the energy go? *Earth System Science Data*, *12*(3), 2013–2041. https://doi.org/10.5194/essd-12-2013-2020

Vu, B. L., Stegner, A., & Arsouze, T. (2018). Angular momentum eddy detection and tracking algorithm (AMEDA) and its application to coastal eddy formation. *Journal of Atmospheric and Oceanic Technology*, *35*(4), 739–762. https://doi.org/10.1175/JTECH-D-17-0010.1

Wong, A. P. S., & Johnson, G. C. (2003). South Pacific eastern subtropical mode water. *Journal of Physical Oceanography*, *33*(7), 1493–1509. https://doi.org/10.1175/1520-0485(2003)033<1493:SPESMW>2.0.CO;2

Wu, B., Lin, X., & Yu, L. (2020). North Pacific subtropical mode water is controlled by the Atlantic multidecadal variability. *Nature Climate Change*, *10*(3), 238–243. https://doi.org/10.1038/s41558-020-0692-5

Xu, L., Li, P., Xie, S.-P., Liu, Q., Liu, C., & Gao, W. (2016). Observing mesoscale eddy effects on mode-water subduction and transport in the North Pacific. *Nature Communications*, *7*(1), 10505. https://doi.org/10.1038/ncomms10505

Xu, L., Xie, S.-P., Liu, Q., Liu, C., Li, P., & Lin, X. (2017). Evolution of the North Pacific subtropical mode water in anticyclonic eddies. *Journal of Geophysical Research: Oceans*, *122*(12), 10118–10130. https://doi.org/10.1002/2017JC013450

Yasuda, T., & Hanawa, K. (1997). Decadal changes in the mode waters in the midlatitude North Pacific. *Journal of Physical Oceanography*, *27*(6), 858–870. https://doi.org/10.1175/1520-0485(1997)027<0858:DCITMW>2.0.CO;2

Yu, L., Jin, X., & Weller, R. (2008). *Multidecade global flux datasets from the objectively analyzed air-sea fluxes (oaflux) project: Latent and sensible heat fluxes, ocean evaporation, and related surface meteorological variables*. OAFlux Project Technical Report.